

NEP_MiniMax: An Approach for NEPs Based on Matrix-valued Minimax Approximations

Chenkun Zhang* Jiawei Gu[†] Lei-Hong Zhang[‡]

March 17, 2026

Abstract

We propose NEP_MiniMax, a novel computational method for solving nonlinear eigenvalue problems (NEPs) $T(\lambda)\mathbf{u} = \mathbf{0}$ on compact continua $\Omega \subset \mathbb{C}$. The method combines two key components: (1) a rational minimax approximation scheme where the m-d-Lawson algorithm constructs a minimax rational approximation for the vector-valued function from $T(x)$'s split form, yielding a matrix-valued rational approximation $R^*(x) = P^*(x)/q^*(x) \approx T(x)$, and (2) a structure-exploiting linearization technique. The minimax approximation guarantees uniform accuracy while generally keeping $R^*(x)$ pole-free in Ω . Eigenpairs are then computed by solving a polynomial eigenvalue problem $P^*(\lambda)\mathbf{u} = \mathbf{0}$ via a strong linearization that exactly preserves eigenvalue multiplicities. Numerical experiments on benchmarks from the NLEVP collection demonstrate competitiveness with state-of-the-art methods (e.g., Beyn, NLEIGS, SV-AAA) in efficiency and accuracy, with theoretical error bounds directly relating eigenpair approximations to the rational approximation quality.

Key words. Nonlinear eigenvalue problem, minimax approximation, rational Krylov method, matrix pencil linearization, Lawson's algorithm, m-d-Lawson iteration.

AMS subject classifications. 65F15, 65H17, 41A20, 65D15

*School of Mathematical Sciences, Soochow University, Suzhou 215006, Jiangsu, China. Email: 19816896524@163.com.

[†]School of Mathematical Sciences, Soochow University, Suzhou 215006, Jiangsu, China. Email: 20244207049@stu.suda.edu.cn.

[‡]Corresponding author. School of Mathematical Sciences, Soochow University, Suzhou 215006, Jiangsu, China. This work was supported in part by the National Natural Science Foundation of China (NSFC-12471356, NSFC-12371380), Jiangsu Shuangchuang Project (JSSCTD202209) and Academic Degree and Postgraduate Education Reform Project of Jiangsu Province. Email: longzlh@suda.edu.cn.

Contents

1	Introduction	2
2	Computing a rational minimax approximant ξ^*	6
2.1	The dual problem of (1.5)	7
2.2	Optimality for the dual objective function	9
2.3	The m-d-Lawson iteration	10
3	Error bound analysis	11
4	Linearization and the framework of NEP_MiniMax	13
4.1	V+A basis and the representation of $P^*(x)$	14
4.2	A linearization of $P^*(x)$	15
4.3	The linearization is strong	16
4.4	The framework of NEP_MiniMax for NEP (1.1)	20
5	Solving the resulting large-scale matrix pencils	21
5.1	Rational filter for matrix pencil	21
5.2	Exploiting block structure in the shift-invert systems	23
5.3	The CORK framework	24
6	Numerical experiments	26
7	Conclusion	34

1 Introduction

Let $\Omega \subset \mathbb{C}$ be a compact Jordan domain whose boundary $\Gamma := \partial\Omega$ is a simple Jordan curve. Consider a continuous matrix-valued function $T : \Omega \rightarrow \mathbb{C}^{n \times n}$ that is analytic in the interior of Ω (i.e., each matrix entry $T_{ij}(x)$ is continuous on Ω and analytic in $\text{int}(\Omega)$). In this paper, we consider the nonlinear eigenvalue problem (NEP) of finding $(\lambda, \mathbf{u}) \in \Omega \times (\mathbb{C}^n \setminus \{\mathbf{0}\})$ such that

$$T(\lambda)\mathbf{u} = \mathbf{0}. \tag{1.1}$$

Here, λ is an eigenvalue of T and \mathbf{u} is the corresponding right eigenvector; (λ, \mathbf{u}) is a right eigenpair of $T(x)$. The spectrum of T in Ω , denoted $\Lambda(T)$, is the set of all eigenvalues lying in Ω . A left eigenpair $(\lambda, \tilde{\mathbf{u}})$ is the one satisfying $\tilde{\mathbf{u}}^H T(\lambda) = \mathbf{0}^H$ for $\tilde{\mathbf{u}} \in \mathbb{C}^n \setminus \{\mathbf{0}\}$. Since left eigenpairs of $T(x)$ can be derived from right eigenpairs of $T(x)^H$, we focus on computing right eigenpairs. As the general setting of NEP in [18], we assume $T(x)$ admits a split form

$$T(x) = \sum_{i=1}^s t_i(x) E_i \tag{1.2}$$

where $t_i : \Omega \rightarrow \mathbb{C}$ is continuous and is analytic in $\text{int}(\Omega)$, and $E_i \in \mathbb{C}^{n \times n}$ is a constant matrix for $i = 1, \dots, s$.

The NEP in the form of (1.2) arises in numerous computational science and engineering disciplines, such as acoustics, control theory, fluid mechanics, and structural mechanics. For a thorough review of applications and state-of-the-art numerical methods as of 2007, we refer readers to [18]. Furthermore, in 2013, [5] provides a MATLAB-based benchmark collection NLEVP that currently contains approximately 80 test problems from various application domains. This comprehensive library encompasses polynomial eigenvalue problems, rational eigenvalue problems, as well as more general nonlinear eigenvalue problems. Owing to its unified interface for diverse NEPs and customizable problem generation parameters, NLEVP has emerged as an essential resource for algorithm development and numerical validation in the field of NEP.

Numerical methods for NEPs can be broadly categorized into four classes: linearization-based methods, iterative projection methods, contour integral-based methods, and Newton-type methods. Linearization-based methods, e.g., [29, 35, 41, 42], leverage the fact that polynomial [31, 32] and rational NEPs [38] can often be transformed into generalized eigenvalue problems (GEPs). For general NEPs of the form (1.2), rational or polynomial approximation techniques (including interpolation and numerical approximation) applied to the nonlinear terms $t_i(x)$ yield tractable polynomial/rational eigenvalue problems. Iterative projection methods (e.g., [39, 43]), including nonlinear Arnoldi and Jacobi-Davidson approaches, extend classical linear eigensolvers by projecting NEP onto carefully constructed subspaces—these excel in large-scale settings through adaptive restarting and repeated linear solves. Contour integral-based methods such as those in [2, 6, 7, 12, 14, 30, 36], exemplified by Beyn’s method and the FEAST framework, employ complex analysis to extract eigenvalues within specified regions via contour integration, avoiding full linearization while targeting interior eigenvalues efficiently. Newton-type methods [13, 23, 24, 25, 26, 33, 37] provide locally superlinear convergence through iterative refinement of eigenvalue-eigenvector pairs, particularly effective for smooth nonlinearities.

In this paper, we focus on computing all eigenvalues within Ω , and our proposed method can be viewed as a new linearization-based method by employing recently developments on rational minimax approximations for vector-valued (or matrix-valued) functions [54] and the related m-d-Lawson iteration. According to the splitting form (1.2), we decouple the treatment of analytic functions t_i from constant matrices E_i by computing an ideal rational vector-valued function $\boldsymbol{\xi}^{\text{best}}(x)$ through

$$\boldsymbol{\xi}^{\text{best}}(x) := [r_1^{\text{best}}(x), \dots, r_s^{\text{best}}(x)]^T := \arg \min_{\boldsymbol{\xi} \in \mathcal{R}_s} \sup_{x \in \Omega} \|[t_1(x), \dots, t_s(x)]^T - \boldsymbol{\xi}(x)\|_2, \quad (1.3)$$

and then construct a rational NEP problem with $R^{\text{best}}(x) = \sum_{i=1}^s r_i^{\text{best}}(x)E_i \approx T(x)$, where

$$\mathcal{R}_s := \left\{ \boldsymbol{\xi}(x) = \begin{bmatrix} r_1(x) \\ \vdots \\ r_s(x) \end{bmatrix} \left| r_i(x) = \frac{p_i(x)}{q(x)}, p_i \in \mathbb{P}_{n_i}, 0 \neq q \in \mathbb{P}_d \right. \right\}, \quad (1.4)$$

$n_i \geq 0$ and $d \geq 0$ are prescribed integers. The i th function $r_i(x) = \frac{p_i(x)}{q(x)}$ of $\boldsymbol{\xi}(x)$ is said to be a rational function of type (n_i, d) , where $p_i \in \mathbb{P}_{n_i}$ is the i th entry of a vector-valued polynomial $\mathbf{p} : \mathbb{C} \rightarrow \mathbb{C}^s$. Since each entry $t_i(x)$ is analytic in its interior and continuous on the boundary $\partial\Omega$, the maximum Frobenius norm principle holds:

$$\sup_{x \in \Omega} \|[t_1(x), \dots, t_s(x)]^T - \boldsymbol{\xi}(x)\|_2$$

is attained on $\partial\Omega$ for any $\boldsymbol{\xi}(x) \in \mathcal{R}_s$ with poles outside Ω (see Theorem 1 in [10]). Consequently, solving (1.3) with carefully chosen boundary nodes $\mathcal{X} = \{x_j\}_{j=1}^m \subset \partial\Omega$ with

$$m \geq \max_{1 \leq i \leq s} (n_i + d + 2)$$

provides an efficient numerical approach for computing minimax rational approximants on Ω . This is realized by the m-d-Lawson iteration [54]. Specifically, we compute an approximant $\boldsymbol{\xi}^* \approx \boldsymbol{\xi}^{\text{best}}$ from the discrete rational minimax approximation

$$\boldsymbol{\xi}^*(x) := [r_1^*(x), \dots, r_s^*(x)]^T := \arg \min_{\boldsymbol{\xi} \in \mathcal{R}_s} \sup_{x \in \mathcal{X}} \|[t_1(x), \dots, t_s(x)]^T - \boldsymbol{\xi}(x)\|_2, \quad (1.5)$$

and form

$$R^*(x) = \sum_{i=1}^s r_i^*(x)E_i \approx R^{\text{best}}(x), \quad (1.6)$$

where $r_i^*(x) = p_i^*(x)/q^*(x)$. Thus we can compute the eigenpairs of $R^*(x)$ to approximate the eigenpairs of $T(x)$.

Notably, Walsh's classical result [44, 45] guarantees the existence of a minimax type (n_i, d) rational approximant for t_i that is pole-free within Ω . Although this existence result does not directly carry over to the discrete case (1.5), our numerical experiments show that, in most cases, the approximately rational minimax approximant $\boldsymbol{\xi}^*$, computed via m-d-Lawson, also remains pole-free in the region of interest. Setting $R^* = R^*(x) = \frac{P^*(x)}{q^*(x)} := \frac{1}{q^*(x)} \sum_{i=1}^s p_i^*(x)E_i$, we consequently have $\Omega \cap \Lambda(R^*) = \Omega \cap \Lambda(P^*)$. This equivalence allows us to compute the eigenvalues of the rational matrix function $R^*(x)$ by solving the eigenvalue problem for the matrix polynomial $P^*(x)$ restricted to Ω . For small to moderate dimension n , we employ linearization followed by the QZ algorithm, while for large-scale problems, we utilize filtered subspace iterations [9] and the compact rational

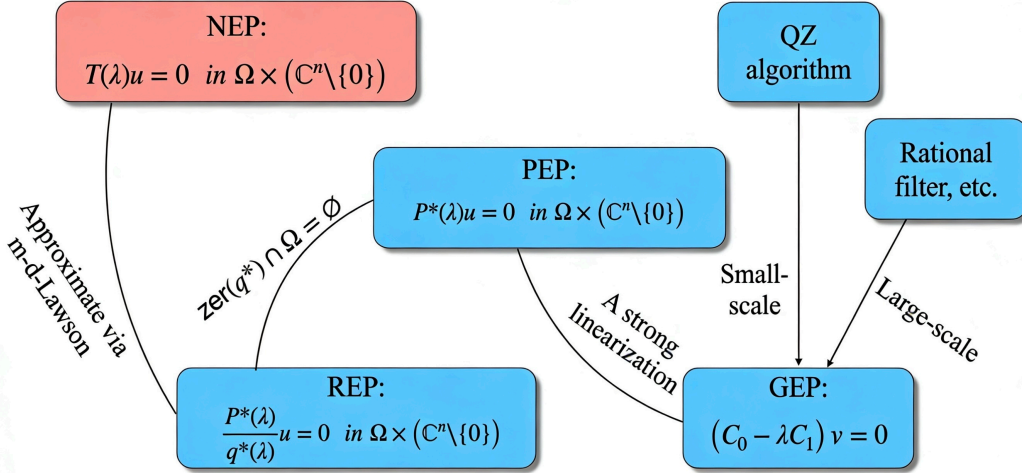


Figure 1.1: Framework of NEP_MiniMax for solving NEPs based on m-d-Lawson and linearization.

Krylov (CORK) framework [42]. The complete framework of our proposed NEP solution approach is illustrated in Figure 1.1.

Paper structure. Building upon the framework illustrated in Figure 1.1, this paper is organized as follows: Section 2 introduces the rational minimax approximation problem (1.5), presenting its dual formulation and the dual-based m-d-Lawson iteration [54]; Section 3 establishes error bounds for $\sup_{x \in \Omega} \|T(x) - R^*(x)\|_F$, providing theoretical justification for our NEP_MiniMax method; Section 4 details linearization techniques for the rational eigenvalue problem $R^*(\lambda)\mathbf{u} = \mathbf{0}$; Section 5 addresses large-scale computation through rational filtering, shift-invert strategies, and the CORK framework [42]; Section 6 validates our approach using NLEVP benchmark problems, demonstrating competitive performance against Byen’s method [6], NLEIGS and SV-AAA [29] in efficiency and accuracy; and concluding remarks are given in Section 7.

Notation. Throughout this paper, $i = \sqrt{-1}$ denotes the imaginary unit and \mathbb{P}_n contains complex polynomials of degree $\leq n$. Vectors appear in bold lowercase, while $\mathbb{C}^{n \times m}$ (resp. $\mathbb{R}^{n \times m}$) denotes all $n \times m$ complex (resp. real) matrices, with $I_n \equiv [\mathbf{e}_1, \dots, \mathbf{e}_n] \in \mathbb{R}^{n \times n}$ being the identity matrix (\mathbf{e}_i is its i th column for $1 \leq i \leq n$). The operator $\text{diag}(\mathbf{x}) = \text{diag}(x_1, \dots, x_m)$ creates diagonal matrices from $\mathbf{x} \in \mathbb{C}^m$, and $\mathbf{x}./\mathbf{y} = [x_1/y_1, \dots, x_m/y_m]^T$ defines element-wise division ($\mathbf{x}, \mathbf{y} \in \mathbb{C}^m$, $y_j \neq 0$). For $A \in \mathbb{C}^{m \times n}$, A^H (resp. A^T) is conjugate (resp. regular) transpose, $\text{span}(A)$ the column space, $\|\cdot\|_F$ the Frobenius norm, and $\text{tr}(\cdot)$ the trace. Following MATLAB notation, $A(\mathcal{J}_1, \mathcal{J}_2)$ denotes the submatrix of A formed by rows indexed by $\mathcal{J}_1 \subseteq [m] =: \{1, \dots, m\}$ and columns indexed by $\mathcal{J}_2 \subseteq [n]$. Finally, $\text{zer}(f)$ denotes zeros of the function f .

2 Computing a rational minimax approximant ξ^*

We begin with a concise overview of the m-d-Lawson algorithm [54] and its application to the target function $T(x)$ in (1.2), with the implementation details following essentially from the theoretical framework developed in [54].

Based on the split form of $T(x)$ (1.2), let

$$\mathbf{t}(x) = \begin{bmatrix} t_1(x) \\ \vdots \\ t_s(x) \end{bmatrix} : \Omega \rightarrow \mathbb{C}^s \quad (2.1)$$

to write (1.3) as

$$\xi^{\text{bset}} := \arg \min_{\xi \in \mathcal{R}_s} \sup_{x \in \Omega} \|\mathbf{t}(x) - \xi(x)\|_2^2, \quad (2.2)$$

where \mathcal{R}_s is defined in (1.4) with prescribed non-negative integers n_i and d . The minimax problem (2.2) is an extension of the classical problem in approximation theory [40] for the complex scale-valued functions. We refer to [52] for the optimality conditions and relations with the dual-based methods for the scale-valued case. As mentioned in Section 1, by the analyticity of each component function $t_i(x)$ in Ω and their continuity on $\partial\Omega$, the maximum Frobenius norm principle applies:

$$\max_{x \in \partial\Omega} \|\mathbf{t}(x) - \xi(x)\|_2 = \max_{x \in \Omega} \|\mathbf{t}(x) - \xi(x)\|_2,$$

where $\xi(x) \in \mathcal{R}_s$ is any rational approximation with poles exterior to Ω (cf. Theorem 1 in [10]). Thus, we resort to numerical methods for its discretized problem by sampling nodes $\mathcal{X} = \{x_j\}_{j=1}^m$ ($m \geq \max_{1 \leq i \leq s} \{n_i + d + 2\}$) in $\partial\Omega$, and consider the discrete rational minimax approximation (1.5) for the vector-valued function $\mathbf{t}(x)$.

To be precise, denote by $\{(x_\ell, \mathbf{t}(x_\ell))\}_{\ell=1}^m$ the sampled data and consider

$$\eta_\infty := \inf_{\xi \in \mathcal{R}_s} \|\mathbf{t}(x) - \xi(x)\|_{\infty, \mathcal{X}}^2, \quad (2.3)$$

where

$$\|\mathbf{t}(x) - \xi(x)\|_{\infty, \mathcal{X}} := \sup_{1 \leq \ell \leq m} \|\mathbf{t}(x_\ell) - \xi(x_\ell)\|_2.$$

Following the traditional treatments of rational approximations for vector-valued or matrix-valued functions [3, 4, 16, 17, 29, 53], we enforce a common denominator $q \in \mathbb{P}_d$ for all entries $r_i(x)$ of ξ in (1.5). In case when the infimum of (2.3) is attainable, we call the function $\xi^* = \frac{1}{q^*} \mathbf{p}^* \in \mathcal{R}_s$ from

$$\xi^* \in \arg \min_{\xi \in \mathcal{R}_s} \|\mathbf{t}(x) - \xi(x)\|_{\infty, \mathcal{X}}^2$$

the rational minimax approximant [40] of $\mathbf{t}(x)$ over \mathcal{X} .

Remark 2.1. We approximate the vector-valued function $\mathbf{t}(x)$ constructed from the components $t_i(x)$ of the split form of $T(x)$, rather than $T(x)$ itself as those in the contour Integral-based methods [2, 6, 7, 12, 14, 30, 36], primarily for computational efficiency. In practice, the dimension parameter n in (1.2) typically dominates s , and the matrices E_i are often large-scale and sparse. This approach yields significant reductions in both computational complexity and storage demands compared to direct min-max approximation of $T(x)$. A detailed error analysis comparing the rational approximation $R^*(x) = \sum_{i=1}^s r_i^*(x)E_i$ with $T(x)$ is provided in Section 3.

2.1 The dual problem of (1.5)

Following [51, 54], to represent a rational function $r_i(x) = \frac{p_i(x)}{q(x)}$, we choose basic function $\{\psi_0(x), \dots, \psi_{n_i}(x)\}$ and $\{\phi_0(x), \dots, \phi_d(x)\}$ to parameter

$$r_i(x) = \frac{p_i(x)}{q(x)} = \frac{[\psi_0(x), \dots, \psi_{n_i}(x)]\mathbf{a}_i}{[\phi_0(x), \dots, \phi_d(x)]\mathbf{b}}, \text{ for some } \mathbf{a}_i \in \mathbb{C}^{n_i+1}, \mathbf{b} \in \mathbb{C}^{d+1}.$$

The monomial basis $\psi_i(x) = \phi_i(x) = x^i$ can usually be used. For the given $\mathcal{X} = \{x_\ell\}_{\ell=1}^m$, we denote by

$$\mathbf{\Psi}_i = \mathbf{\Psi}_i(x_1, \dots, x_m; n_i) := \begin{bmatrix} \psi_0(x_1) & \psi_1(x_1) & \dots & \psi_{n_i}(x_1) \\ \psi_0(x_2) & \psi_1(x_2) & \dots & \psi_{n_i}(x_2) \\ \vdots & \vdots & \ddots & \vdots \\ \psi_0(x_m) & \psi_1(x_m) & \dots & \psi_{n_i}(x_m) \end{bmatrix} \in \mathbb{C}^{m \times (n_i+1)},$$

the associated Vandermonde matrix; therefore,

$$\mathbf{p}_i := [p_i(x_1), \dots, p_i(x_m)]^T = \mathbf{\Psi}_i \mathbf{a}_i \in \mathbb{C}^m.$$

Similarly, we denote by $\mathbf{\Phi} = \mathbf{\Phi}(x_1, \dots, x_m; d) \in \mathbb{C}^{m \times (d+1)}$ the associated Vandermonde matrix for the denominator $q(x)$ at \mathcal{X} , whose (i, j) th entry is $\phi_{j-1}(x_i)$; thus

$$\mathbf{q} := [q(x_1), \dots, q(x_m)]^T = \mathbf{\Phi} \mathbf{b} \in \mathbb{C}^m.$$

Let $\boldsymbol{\xi}(x) = [r_1(x), \dots, r_s(x)]^T \in \mathcal{R}_s$ with each $r_i(x) = p_i(x)/q(x)$ irreducible. If $\|\boldsymbol{\xi}(x)\|_2$ is bounded for any $x \in \mathcal{X}$, then it is easy to see that $q(x) \neq 0$ for any $x \in \mathcal{X}$. Associated with $\boldsymbol{\xi}(x)$ is the maximum error

$$e(\boldsymbol{\xi}) := \max_{x_\ell \in \mathcal{X}} \|\mathbf{t}(x_\ell) - \boldsymbol{\xi}(x_\ell)\|_2^2 = \|\mathbf{t}(x) - \boldsymbol{\xi}(x)\|_{\infty, \mathcal{X}}^2. \quad (2.4)$$

In the following discussion, we assume, without loss of generality, that $\eta_\infty > 0$, i.e., \mathcal{R}_s does not contain an interpolation for $\mathbf{t}(x)$ at $\mathcal{X} = \{x_\ell\}_{\ell=1}^m$.

In [46, 49, 51, 54, 55], by introducing a real variable η , the original minimax problem (2.3) is transformed into the following linearization

$$\begin{aligned} \eta_2 &:= \inf_{\eta \in \mathbb{R}, p_i \in \mathbb{P}_{n_i}, 0 \neq q \in \mathbb{P}_d} \eta \\ \text{s.t.}, \quad &\sum_{i=1}^s |t_i(x_\ell)q(x_\ell) - p_i(x_\ell)|^2 \leq \eta |q(x_\ell)|^2, \quad \forall \ell \in [m]. \end{aligned} \quad (2.5)$$

Unlike the original min-max problem (2.3), (2.5) is a single-level minimization [54]. The following proposition shows that, in general, the two infimums of (2.3) and (2.5) are consistent, and if (2.3) admits a solution, it can be recovered from the linearization (2.5).

Proposition 2.1 ([54]). *Given $m \geq \max_{1 \leq i \leq s} \{n_i + d + 2\}$ distinct nodes $\mathcal{X} = \{x_\ell\}_{\ell=1}^m$ on $\partial\Omega \subseteq \mathbb{C}$, let η_2 be the infimum of (2.5). If $0 \leq d \leq \min_{1 \leq i \leq s} \{n_i\}$, then $\eta_2 = \eta_\infty$; furthermore, in this case, whenever (2.3) has a solution $\boldsymbol{\xi}^* \in \mathcal{R}_s$ with $r_i^* = p_i^*/q^*$ ($1 \leq i \leq s$) irreducible, the tuple $(\eta_\infty, \{p_i^*\}, q^*)$ is a solution of (2.5).*

The dual-based method **m-d-Lawson** for (1.5) is designed for solving the dual problem of (2.5). To this end, by the theory of Lagrange multiplier, the dual function of (2.5) associated with (2.5) is defined by [54]

$$\begin{aligned} d(\mathbf{w}) &= \min_{\mathbf{a}_i \in \mathbb{C}^{n_i+1}, \mathbf{b} \in \mathbb{C}^{d+1}, \sum_{\ell=1}^m w_\ell |q(x_\ell; \mathbf{b})|^2 = 1} \sum_{\ell=1}^m w_\ell \left(\sum_{i=1}^s |t_i(x_\ell)q(x_\ell; \mathbf{b}) - p_i(x_\ell; \mathbf{a}_i)|^2 \right) \\ &= \min_{\mathbf{a} \in \mathbb{C}^N, \mathbf{b} \in \mathbb{C}^{d+1}, \|\sqrt{\mathbf{W}}\boldsymbol{\Phi}\mathbf{b}\|_2 = 1} \left\| \sqrt{\mathbf{W}}_{\otimes} [-\boldsymbol{\Theta}, \mathbf{F}\boldsymbol{\Phi}] \begin{bmatrix} \mathbf{a} \\ \mathbf{b} \end{bmatrix} \right\|_2^2, \end{aligned} \quad (2.6)$$

where $N = \sum_{i=1}^s (n_i + 1)$, $F_i = \text{diag}(t_i(x_1), \dots, t_i(x_m)) \in \mathbb{C}^{m \times m}$,

$$\mathbf{F} = \begin{bmatrix} F_1 \\ \vdots \\ F_s \end{bmatrix} \in \mathbb{C}^{ms \times m}, \quad \boldsymbol{\Theta} = \begin{bmatrix} \boldsymbol{\Psi}_1 & & \\ & \ddots & \\ & & \boldsymbol{\Psi}_s \end{bmatrix} \in \mathbb{C}^{ms \times N}, \quad (2.7)$$

$$\mathbf{a} = [\mathbf{a}_1^T, \dots, \mathbf{a}_s^T]^T \in \mathbb{C}^N, \quad (2.8)$$

and

$$\mathbf{W}_{\otimes} = I_s \otimes W \in \mathbb{C}^{ms \times ms}, \quad W = \text{diag}(\mathbf{w}) \in \mathbb{C}^{m \times m}. \quad (2.9)$$

With the probability simplex $\mathcal{S} := \{\mathbf{w} = [w_1, \dots, w_m]^T \in \mathbb{R}^m : \mathbf{w} \geq 0, \mathbf{w}^T \mathbf{e} = 1\}$ where $\mathbf{e} = [1, \dots, 1]^T \in \mathbb{R}^m$, the following weak duality [54] has been proved:

$$\forall \mathbf{w} \in \mathcal{S}, \quad d(\mathbf{w}) \leq \eta_\infty \implies \max_{\mathbf{w} \in \mathcal{S}} d(\mathbf{w}) \leq \eta_\infty. \quad (2.10)$$

Moreover, by relying on a generalization of Ruttan's sufficient condition [54, Theorem 4.1] and [34], we can also have the following theoretical guarantee for solving the minimax approximant $\boldsymbol{\xi}^*(x)$.

Proposition 2.2. ([54, Theorem 4.1]) *Given $m \geq \max_{1 \leq i \leq s} \{n_i + d + 2\}$ distinct nodes $\mathcal{X} = \{x_\ell\}_{\ell=1}^m$ on $\partial\Omega$, we have weak duality (2.10). Let \mathbf{w}^* be the solution to the dual problem*

$$\max_{\mathbf{w} \in \mathcal{S}} d(\mathbf{w}), \quad (2.11)$$

where $d(\mathbf{w})$ is the Lagrange dual function (2.6), and $(\mathbf{a}^*, \mathbf{b}^*)$ be the associated solution of (2.6) that achieves the minimum $d(\mathbf{w}^*)$, where \mathbf{a}^* contains the coefficient vectors $\mathbf{a}_i^* \in \mathbb{C}^{n_i+1}$ partitioned as in (2.8). Denote

$$\boldsymbol{\xi}^*(x) = \begin{bmatrix} r_1^*(x) \\ \vdots \\ r_s^*(x) \end{bmatrix}, \quad r_i^*(x) = \frac{p_i^*(x)}{q^*(x)}$$

with $p_i^*(x) = [\psi_0(x), \dots, \psi_{n_i}(x)]\mathbf{a}_i^*$, $q^*(x) = [\phi_0(x), \dots, \phi_d(x)]\mathbf{b}^*$. Suppose $q^*(x_\ell) \neq 0$ for all $x_\ell \in \mathcal{X}$. Then if

$$d(\mathbf{w}^*) = \max_{x_\ell \in \mathcal{X}} \|\mathbf{t}(x_\ell) - \boldsymbol{\xi}^*(x_\ell)\|_2^2 := e(\boldsymbol{\xi}^*), \quad (2.12)$$

then strong duality holds, i.e., $d(\mathbf{w}^*) = \eta_\infty$, and $\boldsymbol{\xi}^*(x)$ is the global solution to (2.3). Moreover, when (2.12) holds, then we also have following complementary slackness property:

$$w_\ell^* (e(\boldsymbol{\xi}^*) - \|\mathbf{t}(x_\ell) - \boldsymbol{\xi}^*(x_\ell)\|_2^2) = 0, \quad \forall 1 \leq \ell \leq m. \quad (2.13)$$

Within the dual programming framework of (2.6), we quantify the approximation accuracy of the solution $\boldsymbol{\xi}$ corresponding to minimization (2.6) through the relative error metric:

$$\epsilon(\mathbf{w}) := \left| \frac{d(\mathbf{w}) - e(\boldsymbol{\xi})}{e(\boldsymbol{\xi})} \right|,$$

where \mathbf{w} represents an approximation to the optimal solution \mathbf{w}^* . This error measure naturally serves as the termination criterion for the vector-valued dual Lawson's iteration (denoted as m-d-Lawson) outlined in Algorithm 1.

2.2 Optimality for the dual objective function

To compute the dual function $d(\mathbf{w})$, a minimization problem (2.6) needs to be solved. The following proposition provides the optimality condition for this minimization.

Proposition 2.3. ([54, Proposition 3.1]) *For $\mathbf{w} \in \mathcal{S}$, with notation (2.7), (2.8) and (2.9), we have*

- (i) $\mathbf{c}(\mathbf{w}) = \begin{bmatrix} \mathbf{a}(\mathbf{w}) \\ \mathbf{b}(\mathbf{w}) \end{bmatrix} \in \mathbb{C}^{N+d+1}$ is a solution of (2.6) if and only if it is an eigenvector of the Hermitian positive semi-definite generalized eigenvalue problem $(A_{\mathbf{w}}, B_{\mathbf{w}})$ and $d(\mathbf{w})$ is the smallest eigenvalue satisfying

$$A_{\mathbf{w}}\mathbf{c}(\mathbf{w}) = d(\mathbf{w})B_{\mathbf{w}}\mathbf{c}(\mathbf{w}) \quad \text{and} \quad \mathbf{c}(\mathbf{w})^H B_{\mathbf{w}}\mathbf{c}(\mathbf{w}) = 1, \quad (2.14)$$

where

$$A_{\mathbf{w}} := [-\boldsymbol{\Theta}, \mathbf{F}\boldsymbol{\Phi}]^H \mathbf{W}_{\otimes} [-\boldsymbol{\Theta}, \mathbf{F}\boldsymbol{\Phi}] = \begin{bmatrix} \boldsymbol{\Theta}^H \mathbf{W}_{\otimes} \boldsymbol{\Theta} & -\boldsymbol{\Theta}^H \mathbf{W}_{\otimes} \mathbf{F}\boldsymbol{\Phi} \\ -\boldsymbol{\Phi}^H \mathbf{F}^H \mathbf{W}_{\otimes} \boldsymbol{\Theta} & \boldsymbol{\Phi}^H \mathbf{F}^H \mathbf{W}_{\otimes} \mathbf{F}\boldsymbol{\Phi} \end{bmatrix},$$

$$B_{\mathbf{w}} := [0_{m \times N}, \boldsymbol{\Phi}]^H \mathbf{W} [0_{m \times N}, \boldsymbol{\Phi}] = \begin{bmatrix} 0_{N \times N} & 0_{N \times (d+1)} \\ 0_{(d+1) \times N} & \boldsymbol{\Phi}^H \mathbf{W} \boldsymbol{\Phi} \end{bmatrix};$$

- (ii) the Hermitian matrix $H_{\mathbf{w}} := A_{\mathbf{w}} - d(\mathbf{w})B_{\mathbf{w}}$ is positive semi-definite;

- (iii) let $\sqrt{\mathbf{W}}\boldsymbol{\Phi} = Q_q R_q \in \mathbb{C}^{m \times (d+1)}$ and $\sqrt{\mathbf{W}_{\otimes}}\boldsymbol{\Theta} = Q_p R_p \in \mathbb{C}^{ms \times N}$ be the thin QR factorizations where $Q_q \in \mathbb{C}^{m \times \tilde{n}_2}$, $Q_p \in \mathbb{C}^{ms \times \tilde{n}_1}$, $R_q \in \mathbb{C}^{\tilde{n}_2 \times (d+1)}$, $R_p \in \mathbb{C}^{\tilde{n}_1 \times N}$ with $\tilde{n}_1 = \text{rank}(\sqrt{\mathbf{W}_{\otimes}}\boldsymbol{\Theta})$ and $\tilde{n}_2 = \text{rank}(\sqrt{\mathbf{W}}\boldsymbol{\Phi})$. Then $d(\mathbf{w})$ is the smallest eigenvalue of the following Hermitian positive semi-definite matrix

$$S(\mathbf{w}) := S_{\mathbf{F}} - S_{qp} S_{qp}^H \in \mathbb{C}^{\tilde{n}_2 \times \tilde{n}_2}, \quad (2.15)$$

where

$$S_{\mathbf{F}} = Q_q^H \left(\sum_{i=1}^s |F_i|^2 \right) Q_q \in \mathbb{C}^{\tilde{n}_2 \times \tilde{n}_2}, \quad S_{qp} = Q_q^H \mathbf{F}^H Q_p \in \mathbb{C}^{\tilde{n}_2 \times \tilde{n}_1},$$

with $|F_i| = \text{diag}(|t_i(x_1)|, \dots, |t_i(x_m)|) \in \mathbb{C}^{m \times m}$. Moreover, $\sqrt{d(\mathbf{w})}$ is the smallest singular value of $(I - Q_p Q_p^H) \mathbf{F} Q_q \in \mathbb{C}^{ms \times \tilde{n}_2}$ with the associated singular vector $\hat{\mathbf{b}} = R_q \mathbf{a}(\mathbf{w})$. Also, $R_p \mathbf{a}(\mathbf{w}) = S_{qp}^H \hat{\mathbf{b}}$.

2.3 The m-d-Lawson iteration

In the dual programming framework, Lawson's iteration has been established as an effective method for solving the dual problem (2.11) [54]. Algorithm 1 presents its procedure for the vector-valued rational minimax approximation¹, where particular attention must be paid to the numerical stability and accuracy in computing both the dual objective value $d(\mathbf{w}^{(k)})$ as well as the associated vectors $\mathbf{r}_i^{(k)} = \mathbf{p}_i^{(k)} ./ \mathbf{q}^{(k)}$ ($1 \leq i \leq s$) in Step 3. We use the implementation given in [54] where the Vandermonde with Arnoldi (V+A) approach [8, 22, 50] is employed. This results in rational components $r_i^* = p_i^*/q^*$ where the numerator and

¹See https://ww2.mathworks.cn/matlabcentral/fileexchange/181757-m_d_lawson for the MATLAB code of m-d-Lawson.

denominator polynomials are represented not in the monomial basis, but rather through a system of discrete orthogonal polynomials of increasing degree (we call the V+A basis). This representation motivates our development in Section 4 of a strong linearization framework suitable for matrix polynomials expressed in generalized graded bases. The algorithm incorporates weight updates governed by (2.16) (Step 5), with $\beta > 0$ denoting the Lawson exponent (typically initialized at $\beta = 1$). For comprehensive convergence analysis of m-d-Lawson, we direct readers to [54, Section 5].

Algorithm 1 A matrix-valued dual Lawson's iteration (m-d-Lawson) for (2.3)

Input: Given $\{(x_\ell, \mathbf{t}(x_\ell))\}_{\ell=1}^m$ with $x_\ell \in \partial\Omega$, a tolerance for strong duality $\epsilon_r > 0$, the maximum number k_{\maxit} of iterations, a new vector $\mathbf{y} = [y_1, \dots, y_{\tilde{m}}]^T \in \mathbb{C}^{\tilde{m}}$ of nodes;

Output: The evaluations $\boldsymbol{\xi}^*(y_\ell) \in \mathbb{C}^s$ of the rational minimax approximant $\boldsymbol{\xi}^* \in \mathcal{R}_s$ of (2.3) at y_ℓ for $1 \leq \ell \leq \tilde{m}$.

- 1: (Initialization) Let $k = 0$; choose $\mathbf{0} < \mathbf{w}^{(0)} \in \mathcal{S}$ and a tolerance $\epsilon_{\mathbf{w}}$ for weights;
- 2: (Filtering) Remove nodes x_ℓ with $w_\ell^{(k)} < \epsilon_{\mathbf{w}}$;
- 3: compute $d(\mathbf{w}^{(k)})$ and the associated $\mathbf{r}_i^{(k)} = \mathbf{p}_i^{(k)} ./ \mathbf{q}^{(k)}$ according to proposition (2.3);
- 4: (Stop rule and evaluation) Stop either if $k \geq k_{\maxit}$ or

$$\epsilon(\mathbf{w}^{(k)}) := \left| \frac{e(\boldsymbol{\xi}^{(k)}) - d(\mathbf{w}^{(k)})}{e(\boldsymbol{\xi}^{(k)})} \right| < \epsilon_r, \text{ where } e(\boldsymbol{\xi}^{(k)}) = \max_{x_\ell \in \mathcal{X}} \|\mathbf{t}(x_\ell) - \boldsymbol{\xi}^{(k)}(x_\ell)\|_2^2;$$

compute $r_i^*(\mathbf{y}) = p_i^*(\mathbf{y}) ./ q^*(\mathbf{y}) \in \mathbb{C}^{\tilde{m}}$ and $\{\boldsymbol{\xi}^*(y_\ell)\}_{\ell=1}^{\tilde{m}}$;

- 5: (Updating weights) Update the weight vector $\mathbf{w}^{(k+1)}$ according to

$$w_\ell^{(k+1)} = \frac{w_\ell^{(k)} \|\mathbf{t}(x_\ell) - \boldsymbol{\xi}^{(k)}(x_\ell)\|_2^\beta}{\sum_i w_i^{(k)} \|\mathbf{t}(x_i) - \boldsymbol{\xi}^{(k)}(x_i)\|_2^\beta}, \quad \forall \ell, \quad (2.16)$$

and go to step 2 with $k = k + 1$.

3 Error bound analysis

As mentioned earlier in Remark 2.1, we do not directly approximate the larger-scale function $T(x)$, but instead obtain first $\boldsymbol{\xi}^*(x) = [r_1^*(x), \dots, r_s^*(x)]^T$ by computing the best uniform approximation of its component function $\mathbf{t}(x) = [t_1(x), \dots, t_s(x)]^T$ over the region of interest Ω via m-d-Lawson. The resulting $n \times n$ matrix polynomial $R^*(x) = \sum_{i=1}^s r_i^*(x) E_i$ is then regarded as an approximation to the original function $T(x)$. Therefore, it is necessary to conduct a further analysis of the approximation error between $R^*(x)$ and $T(x)$ over

Ω . Before we provide the error estimate between $R^*(x)$ and $T(x)$, the following lemma is essential.

Lemma 3.1. *With the constant matrices $E_i \in \mathbb{C}^{n \times n}$, $i = 1, \dots, s$, define the following linear mapping*

$$\mathcal{A}_{\{E_i\}_i} : \mathbf{z} = [z_1, \dots, z_s]^T \in \mathbb{C}^s \mapsto \sum_{i=1}^s z_i E_i \in \mathbb{C}^{n \times n}. \quad (3.1)$$

Then for each $\mathbf{z} \in \mathbb{C}^s$, we have $\|\mathcal{A}_{\{E_i\}_i}(\mathbf{z})\|_F \leq \sqrt{\|\mathcal{G}_{\{E_i\}_i}\|_2} \cdot \|\mathbf{z}\|_2$, where

$$\mathcal{G}_{\{E_i\}_i} = \begin{bmatrix} \text{tr}(E_1^H E_1) & \dots & \text{tr}(E_s^H E_1) \\ \vdots & \ddots & \vdots \\ \text{tr}(E_1^H E_s) & \dots & \text{tr}(E_s^H E_s) \end{bmatrix} \in \mathbb{C}^{s \times s}. \quad (3.2)$$

Proof. By definition, we have

$$\begin{aligned} 0 &\leq \|\mathcal{A}_{\{E_i\}_i}(\mathbf{z})\|_F^2 \\ &= \text{tr} \left(\left(\sum_{i=1}^s z_i E_i \right)^H \left(\sum_{j=1}^s z_j E_j \right) \right) \\ &= \sum_{i=1}^s \sum_{j=1}^s z_j^H \text{tr}(E_i^H E_j) z_i = \mathbf{z}^H \mathcal{G}_{\{E_i\}_i} \mathbf{z} \leq \|\mathbf{z}\|_2^2 \cdot \|\mathcal{G}_{\{E_i\}_i}\|_2, \end{aligned}$$

leading to the desired result. \square

The following theorem gives an error bound between T and R^* .

Theorem 3.1. *Suppose $\boldsymbol{\xi}^*(x) = [r_1^*(x), \dots, r_s^*(x)]^T$ and $\mathbf{t}(x) = [t_1(x), \dots, t_s(x)]^T$ satisfying $\sup_{x \in \Omega} \|\mathbf{t}(x) - \boldsymbol{\xi}^*(x)\|_2 \leq \epsilon_{\boldsymbol{\xi}}^\Omega$, then*

$$\sup_{x \in \Omega} \|T(x) - R^*(x)\|_F < \sqrt{\|\mathcal{G}_{\{E_i\}_i}\|_2} \cdot \epsilon_{\boldsymbol{\xi}}^\Omega, \quad (3.3)$$

where $R^*(x) = \sum_{i=1}^s r_i^*(x) E_i$, $T(x) = \sum_{i=1}^s t_i(x) E_i$ and $\mathcal{G}_{\{E_i\}_i} \in \mathbb{C}^{s \times s}$ is defined in (3.2).

Proof. Using Lemma 3.1 and with the notation in (3.1), for each $x \in \Omega$,

$$\begin{aligned} \|T(x) - R^*(x)\|_F &= \|\mathcal{A}_{\{E_i\}_i}(\mathbf{t}(x)) - \mathcal{A}_{\{E_i\}_i}(\boldsymbol{\xi}^*(x))\|_F \\ &= \|\mathcal{A}_{\{E_i\}_i}(\mathbf{t}(x) - \boldsymbol{\xi}^*(x))\|_F \\ &\leq \sqrt{\|\mathcal{G}_{\{E_i\}_i}\|_2} \cdot \|\mathbf{t}(x) - \boldsymbol{\xi}^*(x)\|_2 \leq \sqrt{\|\mathcal{G}_{\{E_i\}_i}\|_2} \cdot \epsilon_{\boldsymbol{\xi}}^\Omega. \end{aligned}$$

\square

Corollary 3.1. *Let $\boldsymbol{\xi}^*$, F , R^* and T be as defined in Theorem 3.1, $\mathcal{G}_{\{E_i\}_i}$ as in (3.2), and assume $\sup_{x \in \Omega} \|\mathbf{t}(x) - \boldsymbol{\xi}^*(x)\|_2 < \epsilon_{\boldsymbol{\xi}}^{\Omega}$. Then for any eigenpair (λ, \mathbf{u}) of R^* , where $\lambda \in \Omega$ and $\|\mathbf{u}\|_2 = 1$, it holds $\|T(\lambda)\mathbf{u}\|_2 \leq \sqrt{\|\mathcal{G}_{\{E_i\}_i}\|_2} \cdot \epsilon_{\boldsymbol{\xi}}^{\Omega}$.*

Proof. The assertion can be seen from

$$\begin{aligned} \|T(\lambda)\mathbf{u}\|_2 &= \|(T(\lambda) - R^*(\lambda))\mathbf{u} - R^*(\lambda)\mathbf{u}\|_2 \\ &\leq \|(T(\lambda) - R^*(\lambda))\mathbf{u}\|_2 + \|R^*(\lambda)\mathbf{u}\|_2 \\ &\leq \|T(\lambda) - R^*(\lambda)\|_2 \cdot \|\mathbf{u}\|_2 \leq \sqrt{\|\mathcal{G}_{\{E_i\}_i}\|_2} \cdot \epsilon_{\boldsymbol{\xi}}^{\Omega}, \end{aligned}$$

where the last inequality follows from Theorem 3.1 and the condition $\|\mathbf{u}\|_2 = 1$. \square

Remark 3.1. In practical applications of Algorithm 1, we can prescribe an error threshold $\epsilon_{\boldsymbol{\xi}}^{\mathcal{X}} > 0$ to ensure $\max_{x_{\ell} \in \mathcal{X}} \|\mathbf{t}(x_{\ell}) - \boldsymbol{\xi}^*(x_{\ell})\|_2 < \epsilon_{\boldsymbol{\xi}}^{\mathcal{X}}$. If \mathcal{X} is a sufficiently refined discretization of $\Gamma = \partial\Omega$, $\epsilon_{\boldsymbol{\xi}}^{\mathcal{X}}$ serves as a numerical approximation of $\epsilon_{\boldsymbol{\xi}}^{\Omega}$ from Theorem 3.1. Furthermore, if $\boldsymbol{\xi}^*(x)$ is pole-free in Ω , the maximum modulus principle guarantees that

$$\sup_{x \in \mathcal{X}} \|\mathbf{t}(x) - \boldsymbol{\xi}^*(x)\|_2 \leq \sup_{x \in \partial\Omega} \|\mathbf{t}(x) - \boldsymbol{\xi}^*(x)\|_2 = \sup_{x \in \Omega} \|\mathbf{t}(x) - \boldsymbol{\xi}^*(x)\|_2 \leq \epsilon_{\boldsymbol{\xi}}^{\Omega}.$$

4 Linearization and the framework of NEP_MiniMax

Let

$$\boldsymbol{\xi}^*(x) = [r_1^*(x), \dots, r_s^*(x)]^T = \begin{bmatrix} p_1^*(x) \\ q^*(x) \\ \vdots \\ p_s^*(x) \\ q^*(x) \end{bmatrix}^T,$$

be obtained from (1.5) and

$$R^*(x) = \frac{1}{q^*(x)} \sum_{i=1}^s p_i^*(x) E_i =: \frac{1}{q^*(x)} P^*(x), \quad (4.1)$$

where $P^*(x)$ is a polynomial matrix on Ω . Clearly, every eigenvalue of $R^*(x)$ must also be an eigenvalue of $P^*(x)$, though the converse does not always hold. Importantly, m-d-Lawson delivers an approximately best uniform approximation for $\mathbf{t}(x) = [t_1(x), \dots, t_s(x)]^T$ over Ω . As demonstrated numerically in Section 6, the approximant $\boldsymbol{\xi}^*(x)$ computed via m-d-Lawson is typically pole-free in Ω and on its boundary, i.e., $\text{zer}(q^*) \cap \Omega = \emptyset$. Without loss of generality, we assume hereafter that the scalar polynomial q^* has no zero on Ω . Consequently,

$$\Omega \cap \Lambda(R^*) = \Omega \cap \Lambda(P^*),$$

indicating that the favorable approximation properties of m-d-Lawson allow the rational eigenvalue problem (REP) for R^* to be converted into a polynomial eigenvalue problem (PEP) for P^* . Thus, approximating the eigenpairs of T on Ω reduces to solving

$$P^*(\lambda)\mathbf{u} = 0, \quad (\lambda, \mathbf{u}) \in \Omega \times (\mathbb{C}^n \setminus \{\mathbf{0}\}).$$

To numerically solve the aforementioned PEP, stability considerations are essential. For instance, an implementation of **m-d-Lawson** proposed in [54] utilizes the Vandermonde with Arnoldi (V+A) method [8]. This approach expresses the polynomials $p_i^*(x)$ and $q^*(x)$ in terms of a discrete orthogonal polynomial basis [8, 50, 56] $\{\vartheta_j(x)\}_{j=0}^\gamma$ constructed with respect to the sample nodes \mathcal{X} . In Section 4.2, we develop the corresponding linearization scheme within this basis framework, reducing the problem to a GEP (C_0, C_1) . Furthermore, we rigorously prove in Section 4.3 that this linearization is strong—guaranteeing both eigenvalue preservation and the maintenance of algebraic multiplicities.

4.1 V+A basis and the representation of $P^*(x)$

Let

$$\gamma = \max \left\{ \max_{1 \leq i \leq s} \{n_i\}, d \right\},$$

where $n_i \forall i \in [s]$ and d are the degree specified by the user for approximation of $p_i^*(x)$ and $q^*(x)$ respectively. According to the Vandermonde with Arnoldi (V+A) [8, 50, 56], we have a discrete orthogonal polynomial (V+A) basis $\{\vartheta_j(x)\}_{j=0}^\gamma$ satisfying $\vartheta_j(x) \in \mathbb{P}_j \forall j \in [\gamma]$ and

$$x [\vartheta_0(x), \vartheta_1(x), \dots, \vartheta_\gamma(x)] = [\vartheta_0(x), \vartheta_1(x), \dots, \vartheta_\gamma(x), \vartheta_{\gamma+1}(x)] H, \quad (4.2)$$

where

$$H = \begin{bmatrix} h_{1,1} & h_{1,2} & \dots & \dots & h_{1,\gamma} & h_{1,\gamma+1} \\ h_{2,1} & h_{2,2} & \dots & \dots & h_{2,\gamma} & h_{2,\gamma+1} \\ & h_{3,2} & \dots & \dots & h_{3,\gamma} & h_{3,\gamma+1} \\ & & \ddots & & \vdots & \vdots \\ & & & \ddots & h_{\gamma,\gamma} & h_{\gamma,\gamma+1} \\ & & & & h_{\gamma+1,\gamma} & h_{\gamma+1,\gamma+1} \\ & & & & & h_{\gamma+2,\gamma+1} \end{bmatrix} \in \mathbb{C}^{(\gamma+2) \times (\gamma+1)} \quad (4.3)$$

is an irreducible (i.e., $h_{i+1,i} \neq 0$) upper-Hessenberg matrix obtained from the V+A process [8, 50, 56]. In particular, if the nodes $\mathcal{X} = \{x_j\}_{j=1}^m \subset \mathbb{R}$ are real-valued, the matrix H reduces to a tridiagonal form; moreover, it can be proved using a complex version of the implicit Q theorem [15, Theorem 7.4.2] that this property extends to the complex case when all nodes $\mathcal{X} \subset \mathbb{C}$ lie on a straight line in the complex plane. With this V+A basis,

we can write $p_i^*(x) = \sum_{j=0}^\gamma a_{i,j}^* \vartheta_j(x)$, and consequently

$$P^*(x) = \sum_{i=1}^s \left(\sum_{j=0}^\gamma a_{i,j}^* \vartheta_j(x) \right) E_i = \sum_{j=0}^\gamma \vartheta_j(x) \left(\sum_{i=1}^s a_{i,j}^* E_i \right) =: \sum_{j=0}^\gamma \vartheta_j(x) A_j. \quad (4.4)$$

Remark 4.1. It is worth noting that as long as H is irreducible, $\{\vartheta_i(x)\}_{i=0}^\gamma$ forms a family of polynomials with strictly increasing degrees. That is, $\{\vartheta_i(x)\}_{i=0}^\gamma$ is a degree-graded system. Notably, common bases such as monomial bases and orthogonal polynomial bases (including Chebyshev polynomials) satisfy these recurrence relations as special cases. Consequently, our proposed linearization approach maintains favorable properties while extending applicability to any matrix polynomial expressed in an arbitrary degree-graded basis, thereby generalizing the specific linearization framework developed in [1] for matrix polynomials expressed in bases satisfying three-term recurrence relations.

4.2 A linearization of $P^*(x)$

Now, we construct a linearization of $P^*(x) = \sum_{j=0}^{\gamma} \vartheta_j(x)A_j$ in (4.4). For simplicity, we denote by k_j the coefficient of the highest degree in $\vartheta_j(x)$ with $k_0 = 1$, i.e. $\vartheta_0(x) \equiv 1$. Then by the recurrence relation (4.2), it holds that

$$h_{j+1,j} = \frac{k_{j-1}}{k_j}, \quad j = 1, 2, \dots, \gamma. \quad (4.5)$$

The following lemma plays an important role in constructing the linearization of P^* .

Lemma 4.1. *Define the matrix pencil (C_0, C_1) as follows:*

$$C_0 := \begin{bmatrix} H([\gamma], [\gamma - 1])^T \otimes I_n \\ -k_{\gamma-1}[A_0, A_1, \dots, A_{\gamma-1}] + k_\gamma H([\gamma], \gamma)^T \otimes A_\gamma \end{bmatrix}, \quad C_1 := \begin{bmatrix} I_{(\gamma-1)n} & \\ & k_\gamma A_\gamma \end{bmatrix},$$

where $H([\gamma], [\gamma - 1])$ denotes the submatrix consisting of the first γ rows and first $\gamma - 1$ columns of H , while $H([\gamma], \gamma)$ represents the γ -th column of H as defined in (4.3). Then we have

$$(C_0 - xC_1) \begin{bmatrix} \vartheta_0(x)I_n \\ \vartheta_1(x)I_n \\ \vdots \\ \vartheta_{\gamma-1}(x)I_n \end{bmatrix} = \begin{bmatrix} \mathbf{0} \\ \mathbf{0} \\ \vdots \\ -k_{\gamma-1}P^*(x) \end{bmatrix},$$

or equivalently,

$$(C_0 - xC_1)(\boldsymbol{\vartheta}(x) \otimes I_n) = -k_{\gamma-1}(\mathbf{e}_\gamma \otimes P^*(x)), \quad (4.6)$$

where $\boldsymbol{\vartheta}(x) = [\vartheta_0(x), \dots, \vartheta_{\gamma-1}(x)]^T$.

Proof. By calculations, we obtain

$$(C_0 - xC_1)(\boldsymbol{\vartheta} \otimes I_n) = \begin{bmatrix} (x\vartheta_0 - \sum_{j=1}^2 h_{j,1}\vartheta_{j-1})I_n \\ \vdots \\ (x\vartheta_{\gamma-2} - \sum_{j=1}^{\gamma} h_{j,\gamma-1}\vartheta_{j-1})I_n \\ -k_{\gamma-1} \sum_{j=0}^{\gamma-1} \vartheta_j A_j - k_{\gamma} \left(x\vartheta_{\gamma-1} - \sum_{j=1}^{\gamma} h_{j,\gamma}\vartheta_{j-1} \right) A_{\gamma} \end{bmatrix}. \quad (4.7)$$

With the recurrence relation (4.2), the first $\gamma - 1$ blocks in (4.7) are all 0. Finally, by (4.2) and $h_{\gamma+1,\gamma} = \frac{k_{\gamma-1}}{k_{\gamma}}$, we get

$$-k_{\gamma-1} \sum_{j=0}^{\gamma-1} \vartheta_j(x) A_j - k_{\gamma} \left(x\vartheta_{\gamma-1}(x) - \sum_{j=1}^{\gamma} h_{j,\gamma}\vartheta_{j-1}(x) \right) A_{\gamma} = -k_{\gamma-1} P^*(x)$$

as desired. \square

The next result then reveals the relationship between the eigenvalues of P^* and linear matrix pencil (C_0, C_1) :

Corollary 4.1. *Every finite eigenvalue of P^* is also an eigenvalue of the matrix pencil (C_0, C_1) defined in (4.6).*

Proof. Assume (λ, \mathbf{u}) is an eigenpair of P^* , i.e. $P^*(\lambda)\mathbf{u} = \mathbf{0}$. Using Lemma 4.1, we obtain

$$(C_0 - \lambda C_1)(\boldsymbol{\vartheta}(\lambda) \otimes \mathbf{u}) = -k_{\gamma-1} \mathbf{e}_{\gamma} \otimes (P^*(\lambda)\mathbf{u}) = \mathbf{0}, \quad (4.8)$$

leading to the desired result. \square

Remark 4.2. Through the proof of Corollary 4.1, we find that if (λ, \mathbf{u}) is the eigenpair of P^* , then $(\lambda, \boldsymbol{\vartheta}(\lambda) \otimes \mathbf{u})$ is the eigenpair of the matrix pencil (C_0, C_1) , where $\boldsymbol{\vartheta}(x)$ is defined in (4.6). Indeed, it is easy to check that the opposite is also true. Specifically, if (λ, \mathbf{v}) is an eigenpair of (C_0, C_1) and we write $\mathbf{v} = [\mathbf{v}_1^T, \mathbf{v}_2^T, \dots, \mathbf{v}_{\gamma}^T]^T$. Then λ is an eigenvalue of P^* and \mathbf{v}_1 is the associated eigenvector. Moreover, $\forall i = 2, \dots, \gamma$, \mathbf{v}_i can be obtained from

$$\mathbf{v}_i = \vartheta_{i-1}(\lambda)\mathbf{v}_1, \quad i = 2, 3, \dots, \gamma. \quad (4.9)$$

4.3 The linearization is strong

While Corollary 4.1 provides a method for computing eigenpairs of P^* , a critical question remains: whether $C_0 - \lambda C_1$ defined in (4.6) constitutes a strong linearization [1, Definition 2.1] of $P^*(\lambda)$. This property is particularly important because strong linearizations

preserve the complete spectral information of the original matrix polynomial, including eigenvalue multiplicities [27]. Such preservation is essential for rigorous analysis of eigenvalue distributions, stability properties, and related problems. In this subsection, we will establish this strong linearization property.

For any polynomial $P(\lambda)$ of degree at most γ , we define its reverse polynomial as $P^\#(\lambda) := \lambda^\gamma P(\lambda^{-1})$. The concept of strong linearization is formally characterized as follows:

Definition 4.1. ([1, Definition 2.1]) A $\gamma n \times \gamma n$ linear matrix pencil $\lambda A - B$ is a strong linearization of $n \times n$ regular matrix polynomial $P(\lambda)$ of degree γ if there are unimodular matrix polynomials² $D(\lambda)$ and $G(\lambda)$ such that

$$\begin{bmatrix} P(\lambda) \\ I_{(\gamma-1)n} \end{bmatrix} = D(\lambda)(\lambda A - B)G(\lambda), \quad (4.10)$$

and there are unimodular matrix polynomials $H(\lambda)$ and $K(\lambda)$ such that

$$\begin{bmatrix} P^\#(\lambda) \\ I_{(\gamma-1)n} \end{bmatrix} = H(\lambda)(A - \lambda B)K(\lambda). \quad (4.11)$$

Theorem 4.1. ([1, Theorem 2.2]) *Let $P(\lambda)$ be an $n \times n$ regular matrix polynomial with leading coefficient A_γ (possibly zero) and let $\lambda A - B$ be a $\gamma n \times \gamma n$ linear matrix function. Assume that, for each distinct finite eigenvalue λ_j there exist functions $D_j(\lambda)$ and $G_j(\lambda)$ which are unimodular and analytic on a neighbourhood of λ_j and for which*

$$\begin{bmatrix} P(\lambda) \\ I_{(\gamma-1)n} \end{bmatrix} = D_j(\lambda)(\lambda A - B)G_j(\lambda). \quad (4.12)$$

If A_γ is singular (or zero), assume also that there are functions $D_0(\lambda)$ and $G_0(\lambda)$ which are unimodular and analytic on a neighbourhood of $\lambda = 0$ and for which

$$\begin{bmatrix} P^\#(\lambda) \\ I_{(\gamma-1)n} \end{bmatrix} = D_0(\lambda)(A - \lambda B)G_0(\lambda). \quad (4.13)$$

Then $\lambda A - B$ is a strong linearization of $P(\lambda)$.

Suppose condition (4.10) (or (4.12)) holds without any reference to spectral behavior at infinity (if any). Then, the matrix pencil $\lambda A - B$ is referred to as a weak linearization of the associated polynomial.

The following LU factorization is essential to prove that $\lambda C_1 - C_0$ defined in (4.6) is a strong linearization of $P^*(\lambda)$.

Lemma 4.2. *Let the pencil (C_0, C_1) be given in (4.6).*

² $D(x) : \Omega \rightarrow \mathbb{C}^{n \times n}$ is a unimodular matrix-valued function if $\det(D(x))$ is a nonzero constant over Ω .

(i) Define permutation matrix S as

$$S := \begin{bmatrix} I_n & & & I_n \\ & I_n & & \\ & & \ddots & \\ & & & I_n \end{bmatrix}. \quad (4.14)$$

Then we have

$$(\lambda C_1 - C_0) S = L(\lambda) U(\lambda), \quad (4.15)$$

where

$$U(\lambda) = \begin{bmatrix} I_n & & -\frac{\vartheta_1(\lambda)}{\vartheta_0(\lambda)} I_n \\ & I_n & \vdots \\ & & \ddots & -\frac{\vartheta_{\gamma-1}(\lambda)}{\vartheta_0(\lambda)} I_n \\ & & & I_n \end{bmatrix}, \quad (4.16)$$

$$L(\lambda) = \begin{bmatrix} -h_{2,1} I_n & & & & & \\ (\lambda - h_{2,2}) I_n & -h_{3,2} I_n & & & & \\ \vdots & \vdots & \ddots & & & \\ -h_{2,\gamma-2} I_n & -h_{3,\gamma-2} I_n & \cdots & -h_{\gamma-1,\gamma-2} I_n & & \\ -h_{2,\gamma-1} I_n & -h_{3,\gamma-1} I_n & \cdots & (\lambda - h_{\gamma-1,\gamma-1}) I_n & -h_{\gamma,\gamma-1} I_n & \\ l_{1,\gamma} & l_{2,\gamma} & \cdots & l_{\gamma-2,\gamma} & l_{\gamma-1,\gamma} & l_{\gamma,\gamma} \end{bmatrix}, \quad (4.17)$$

and

$$l_{i,\gamma} = \begin{cases} k_{\gamma-1} A_i - k_\gamma h_{i+1,\gamma} A_\gamma, & i = 1: (\gamma - 2), \\ k_{\gamma-1} A_{\gamma-1} - k_\gamma h_{\gamma,\gamma} A_\gamma + \lambda k_\gamma A_\gamma, & i = \gamma - 1, \\ \frac{1}{\prod_{i=1}^{\gamma-1} h_{i+1,i}} P^*(\lambda), & i = \gamma. \end{cases} \quad (4.18)$$

(ii) $\lambda C_1 - C_0 = L^\#(\lambda) U^\#(\lambda)$, where

$$U^\#(\lambda) = \begin{bmatrix} I_n & -\frac{\vartheta_0(\lambda)}{\vartheta_1(\lambda)} I_n & & & \\ & I_n & \ddots & & \\ & & & \ddots & \\ & & & & -\frac{\vartheta_{\gamma-2}(\lambda)}{\vartheta_{\gamma-1}(\lambda)} I_n \\ & & & & I_n \end{bmatrix}, \quad (4.19)$$

Consequently, we obtain $\begin{bmatrix} I_{(\gamma-1)n} & \\ & P^*(\lambda) \end{bmatrix} = D(\lambda)(\lambda C_1 - C_0)G(\lambda)$, where $D(\lambda) = \tilde{L}^{-1}(\lambda)$ and $G(\lambda) = SU^{-1}(\lambda)$ are both analytic and invertible at all finite eigenvalues of $P^*(\lambda)$. By Theorem 4.1, $\lambda C_1 - C_0$ is thus a weak linearization of $P^*(\lambda)$.

For the strong linearization, we next examine its behavior under reversal by considering the reverse polynomial:

$$P^\#(\lambda) := (P^*(\lambda))^\# = \lambda^\gamma P^*(\lambda^{-1}).$$

Following Theorem 4.1, we must construct matrix functions $H(\lambda)$ and $K(\lambda)$ that are analytic and nonsingular near $\lambda = 0$ and satisfy the decomposition

$$\begin{bmatrix} I_{(\gamma-1)n} & \\ & P^\#(\lambda) \end{bmatrix} = H(\lambda)(C_1 - \lambda C_0)K(\lambda).$$

Step 1 (Reverse Factorization): By Lemma 4.1(ii), the pencil admits a factorization $\lambda C_1 - C_0 = L^\#(\lambda)U^\#(\lambda)$, where $L^\#(\lambda)$ and $U^\#(\lambda)$ are given in (4.20) and (4.19). Applying the substitution $\lambda \mapsto \lambda^{-1}$, we derive $C_1 - \lambda C_0 = \lambda L^\#(\lambda^{-1})U^\#(\lambda^{-1})$, which yields the reverse LU-factors:

$$L_1(\lambda) = \lambda L^\#(\lambda^{-1}), \quad U_1(\lambda) = U^\#(\lambda^{-1}).$$

Step 2 (Local Analysis at $\lambda = 0$): To ensure analyticity near $\lambda = 0$, we define $K(\lambda) = U_1^{-1}(\lambda)$. A modified matrix $\tilde{L}_1(\lambda)$, obtained by replacing the last block entry $L_1(\lambda)$ with

$$\frac{\vartheta_0(\lambda^{-1})}{\lambda^{\gamma-1}\vartheta_{\gamma-1}(\lambda^{-1})\prod_{k=1}^{\gamma-1}h_{k+1,k}}I_n,$$

ensuring $\det(\tilde{L}_1(\lambda)) \equiv \text{const.} \neq 0$. Setting $H(\lambda) = \tilde{L}_1^{-1}(\lambda)$, one can directly verify that (4.3) holds.

We now analyze the properties of $H(0)$ and $K(0)$. As established by [1, Theorem 3.1], $K(\lambda)$ is analytic and invertible at $\lambda = 0$, so we focus on examining $H(\lambda)$ near the origin. Considering the structure of $L_1(\lambda)$ derived from (4.20) and (4.21), we observe that as $\lambda \rightarrow 0$, the diagonal entries are $O(1)$ and off-diagonal entries are at least $O(\lambda)$ (note the exceptional (γ, γ) block in (4.3) exhibits different scaling behavior). Together, these properties guarantee that both $H(\lambda)$ and $K(\lambda)$ remain analytic and invertible in a neighborhood of $\lambda = 0$, thereby completing the proof. \square

4.4 The framework of NEP_MiniMax for NEP (1.1)

We now describe the framework of our proposed NEP_MiniMax (Algorithm 2) for solving NEP (1.1), leveraging m-d-Lawson and linearization techniques. Letting $\mathbf{n} = [n_1, \dots, n_s]^T$, we compute

$$\boldsymbol{\xi}^* = \text{m-d-Lawson}(\mathbf{t}, \mathcal{X}, \mathbf{n}, d)$$

to obtain approximately the best rational approximation $\boldsymbol{\xi}^*(x) = [p_1^*(x), \dots, p_s^*(x)]^\top / q^*(x)$ of $\mathbf{t}(x)$ over the sample set $\mathcal{X} = \{x_\ell\}_{\ell=1}^m$, where each pair $(p_i^*(x), q^*(x))$ has type (n_i, d) . For simplicity, we set $n_i = d$ for rational approximation and $n_i = k$ (with $d = 0$) for polynomial approximation. During the approximation stage (lines 2–5 of Algorithm 2), the degree is iteratively increased until $\sqrt{e(\boldsymbol{\xi}^*)}$ satisfies $\sqrt{e(\boldsymbol{\xi}^*)} < \epsilon_{\boldsymbol{\xi}}^{\mathcal{X}}$. For eigenvalue computation, small-scale matrix pencils (C_0, C_1) are resolved using MATLAB’s `eig` function, whereas large-scale problems necessitate specialized methods [9, 35, 39] to mitigate computational demands. The cross-product structure of (C_0, C_1) (4.6) in our framework facilitates efficient eigenvalue computation, as elaborated in the subsequent section.

Algorithm 2 The framework of NEP_MiniMax for (1.1)

Input: Given a matrix-valued function $T(x) = \sum_{i=1}^s t_i(x)E_i$ with sample $\mathcal{X} = \{x_\ell\}_{\ell=1}^m \subset \partial\Omega$, a tolerance $\epsilon_{\boldsymbol{\xi}}^{\mathcal{X}} > 0$, the maximum degree d_{\max} for approximation.

Output: The computed eigenpairs $(\lambda^*, \mathbf{u}^*)$ of $T(x)$.

- 1: Let $\mathbf{t}(x) = [t_1(x), \dots, t_s(x)]^\top$;
 - 2: **for** $k = 1$ to d_{\max} **do**
 - 3: $\boldsymbol{\xi}^* = \text{m-d-Lawson}(\mathbf{t}, \mathcal{X}, k\mathbf{e}, k)$;
 - 4: Stop if $\sqrt{e(\boldsymbol{\xi}^*)} < \epsilon_{\boldsymbol{\xi}}^{\mathcal{X}}$;
 - 5: **end for**
 - 6: Let $R^*(x) = \frac{1}{q^*(x)} \sum_{i=1}^s p_i^*(x)E_i$ and construct pencil (C_0, C_1) according to (4.6);
 - 7: Compute (C_0, C_1) ’s eigenpairs $(\lambda^*, \mathbf{v}^*)$, then $\mathbf{u}^* = \mathbf{v}^*(1 : n, :)$.
-

5 Solving the resulting large-scale matrix pencils

As previously discussed, the eigenvalue problem for an $n \times n$ matrix polynomial $P^*(\lambda)$ of degree γ can be reformulated as a GEP (C_0, C_1) —defined in (4.6)—with dimension $\gamma n \times \gamma n$. For small-to-medium-scale problems (where γn is computationally tractable), one can directly apply the QZ algorithm to (C_0, C_1) to compute all eigenvalues. For large-scale problems, however, memory-efficient subspace iteration methods [35, 39] or rational filtering techniques [9]—the latter defined on a target region Ω —become necessary alternatives. Additionally, when the matrix pencil exhibits structured forms, more specialized approaches are available. In particular, [42] demonstrates that for pencils with Kronecker product structure, the compact rational Krylov method (CORK) provides an effective framework for eigenvalue computation.

5.1 Rational filter for matrix pencil

Recall that $\Omega \subset \mathbb{C}$ is a compact Jordan domain with boundary $\Gamma = \partial\Omega$ consisting of a simple Jordan curve. The indicator function of Ω can be expressed through contour

integration [19, 48] as

$$\rho(x) = \frac{1}{2\pi i} \oint_{\Gamma} \frac{1}{z-x} dz = \begin{cases} 1, & x \in \text{int}(\Omega), \\ 0, & x \notin \Omega, \end{cases} \quad (5.1)$$

which naturally defines a rational filter for Ω . The filter $\rho(x)$ enables selective extraction of eigenvalues within Ω (excluding Γ). Indeed, for any diagonalizable matrix pencil (A, B) satisfying $AX = BX\Lambda$, where Λ contains the eigenvalues on its diagonal, the filtered matrix becomes [48]

$$\rho(B^{-1}A) = X\mathbf{1}_{\Omega}(\Lambda)X^{-1},$$

with $\mathbf{1}_{\Omega}(\cdot)$ denoting the eigenvalue indicator function. Crucially, $\rho(B^{-1}A)$ projects onto $\text{span}\{\mathbf{u}_1, \dots, \mathbf{u}_k\}$, where $\{\mathbf{u}_i\}_{i=1}^k$ are eigenvectors corresponding to eigenvalues of (A, B) lying within Ω . Remarkably, this contour integral approach remains valid even for defective non-Hermitian pencils [48] and yields the method HFEAST [47]. These results underlie the SIF (Subspace Iteration with Filter) method (Algorithm 3) for computing eigenvalues of large-scale pencils (C_0, C_1) .

Algorithm 3 Subspace iteration with filter [9, 47]

Input: A matrix pencil (C_0, C_1) , Ω , number of columns \tilde{n} , shift σ .

Output: All approximate eigenpairs $(\tilde{\lambda}_i, \tilde{\mathbf{y}}_i)$, $\tilde{\lambda}_i \in \Omega$.

- 1: Generate random $Y \in \mathbb{C}^{n \times \tilde{n}}$;
 - 2: **while** not converge **do**
 - 3: $U = \rho(C_1^{-1}C_0)Y$;
 - 4: $V = \text{orth}(U)$;
 - 5: $W = \text{orth}((C_0 - \sigma C_1)V)$;
 - 6: $\{(\tilde{\lambda}_i, \tilde{\mathbf{x}}_i)\}_{i=1}^{\tilde{n}} = \text{eig}(W^H C_0 V, W^H C_1 V)$;
 - 7: $\tilde{\mathbf{y}}_i = V\tilde{\mathbf{x}}_i$, and $Y = [\tilde{\mathbf{y}}_1, \dots, \tilde{\mathbf{y}}_{\tilde{n}}]$;
 - 8: **end while**
-

Remark 5.1. We have some explanations on Algorithm 3:

- (1) In Line 4, $U = \text{orth}(V)$ denotes an orthonormal basis for the range of V , typically computed via thin QR decomposition of V ; the same applies for Line 5. The left eigenspace basis W is constructed as $W = \text{orth}(C_0 V - \sigma C_1 V)$, where σ is a shift parameter chosen to avoid the eigenvalues of (C_0, C_1) . For implementation details, we refer to the HFEAST algorithm [47].
- (2) The eigenpairs $(\tilde{\lambda}_i, \tilde{\mathbf{x}}_i)$ of the reduced $\tilde{n} \times \tilde{n}$ generalized eigenvalue problem (Line 6) can be computed using MATLAB's `eig`, as \tilde{n} is typically small enough for dense direct methods.
- (3) Under exact arithmetic conditions, a single iteration of the rational filter $\rho(C_1^{-1}C_0)$ applied to Y would yield a subspace V that exactly spans the desired invariant subspace.

In such idealized scenarios, the computed Ritz pairs $(\tilde{\lambda}_i, \tilde{\mathbf{y}}_i)$ from the reduced problem precisely coincide with eigenpairs of the original pencil (C_0, C_1) .

We emphasize that the filter $\rho(x)$ defined in (5.1) involves a contour integral and thus requires numerical approximation in practice. For the special case when Γ is a circular contour with center c and radius r , we parameterize it using $c + re^{i\theta}$ ($\theta \in [0, 2\pi)$), reducing (5.1) to a one-dimensional integral amenable to standard quadrature methods. Following the approach in [9], we employ the k -point trapezoidal rule, which yields the discrete approximation

$$\zeta_{c,r,k}(x) = \sum_{j=1}^k \frac{g_j^{(k)}}{s_j^{(k)} - x}, \quad (5.2)$$

where the poles $s_j^{(k)}$ and weights $g_j^{(k)}$ are given by

$$s_j^{(k)} = c + re^{i\theta_j^{(k)}}, \quad g_j^{(k)} = \frac{r}{k} e^{i\theta_j^{(k)}}, \quad \theta_j^{(k)} = \frac{(2j-1)\pi}{k}. \quad (5.3)$$

Consequently, the action of the filter on Y is approximated as

$$\rho(C_1^{-1}C_0)Y \approx \zeta_{c,r,k}(C_1^{-1}C_0)Y = \sum_{j=1}^k g_j^{(k)} (s_j^{(k)}C_1 - C_0)^{-1} C_1 Y. \quad (5.4)$$

For rigorous error analysis, convergence rates, and generalizations to composite quadrature rules, we refer readers to [9].

5.2 Exploiting block structure in the shift-invert systems

The solution of (5.4) involves solving k linear systems of dimension $\gamma n \times \gamma n$, which inherently depends on shift-invert iteration. Specifically, for a given shift μ and initial matrix $Y \in \mathbb{C}^{\gamma m \times \tilde{n}}$, each shift-invert step computes Z via the linear system:

$$(\mu C_1 - C_0)Z = C_1 Y. \quad (5.5)$$

While a standard implementation requires solving a full $\gamma n \times \gamma n$ system per iteration, our framework leverages the structure of the pencil (C_0, C_1) —particularly the block LU decomposition in (4.15)—to reduce the computational cost to solving (5.5).

By the LU factorization from Lemma 4.2(i), (5.5) becomes equivalent to

$$(L(\mu)U(\mu))S^T Z = C_1 Y,$$

where $L(\mu)$ and $U(\mu)$ are derived by substituting $\lambda = \mu$ into $L(\lambda)$ in (4.17) and $U(\lambda)$ in (4.16), respectively. Defining $X := U(\mu)S^T Z$, we solve for Z via

$$S^T Z = U^{-1}(\mu)X, \quad L(\mu)X = C_1 Y.$$

Partition $X = [X_1^T, \dots, X_\gamma^T]^T$ and $Y = [Y_1^T, \dots, Y_\gamma^T]^T$, with $X_i, Y_i \in \mathbb{C}^{n \times \tilde{n}}$. Using the structures of C_1 , $U(\mu)$, and $L(\mu)$, (4.6), (4.16), (4.17) and noting $\vartheta_0 \equiv 1$, direct computation yields

$$S^T Z = \begin{bmatrix} X_1 + \vartheta_1(\mu)X_\gamma \\ \vdots \\ X_{\gamma-1} + \vartheta_{\gamma-1}(\mu)X_\gamma \\ X_\gamma \end{bmatrix}, \quad (5.6)$$

while X is resolved through

$$\begin{cases} X_1 = -Y_1/h_{2,1}, & X_2 = -(Y_2 - (\mu - h_{2,2})X_1)/h_{3,2}, \\ X_i = -\left(Y_i - (\mu - h_{i,i})X_{i-1} + \sum_{j=1}^{i-2} h_{j+1,i}X_j\right)/h_{i+1,i}, & i = 3, \dots, \gamma - 1, \\ P^*(\mu) X_\gamma = \left(\Pi_{i=1}^{\gamma-1} h_{i+1,i}\right) \left(k_\gamma A_\gamma Y_\gamma - \sum_{i=1}^{\gamma-1} l_{i,\gamma} X_i\right), \end{cases} \quad (5.7)$$

where $\{l_{i,\gamma}\}_{i=1}^{\gamma-1} \subset \mathbb{C}^{n \times n}$ is defined in (4.18). Crucially, the dominant cost in computing Z in (5.5) reduces to solving n -dimensional systems for X_γ .

By combining trapezoidal quadrature and block LU decomposition, we develop an efficient method for computing $U = \rho(C_1^{-1}C_0)Y$ (Line 3, Algorithm 3), as outlined in Algorithm 4. Notably, Algorithm 3 maintains a fixed quadrature order k across iterations. This choice ensures that the set of linear systems $P^*(s_j^{(k)})$ ($j = 1, \dots, k$) remains invariant, allowing their pre-factorization prior to subspace iteration—significantly accelerating linear system solves within each iteration. Furthermore, Line 3 of Algorithm 4 reveals that the computations of G_j ($j = 1, \dots, k$) are fully independent. This property makes the approximation

$$\rho(C_1^{-1}C_0)Y \approx \sum_{j=1}^k g_j^{(k)} \left(s_j^{(k)}C_1 - C_0\right)^{-1} C_1 Y$$

inherently parallelizable, enabling efficient exploitation of parallel computing resources.

5.3 The CORK framework

Another useful approach for the solving large-scale matrix pair (C_0, C_1) in (4.6) is the compact rational Krylov method (CORK) [42]. This approach centers on a matrix-valued function of the form

$$\tilde{P}(x) = \sum_{i=0}^{\gamma-1} (\tilde{A}_i - x\tilde{B}_i) \varphi_i(x), \quad \tilde{A}_i, \tilde{B}_i \in \mathbb{C}^{n \times n}, \quad (5.8)$$

where $\varphi_i : \mathbb{C} \rightarrow \mathbb{C}$ are polynomial or rational functions satisfying the linear relation

$$(M - xN) \varphi(x) = \mathbf{0}, \quad (5.9)$$

Algorithm 4 A practical method for computing $\rho(C_1^{-1}C_0)Y$

Input: The order k of the trapezoidal rule.

Output: $\zeta_{c,r,k}(C_1^{-1}C_0)Y = \sum_{j=1}^k g_j^{(k)} (s_j^{(k)}C_1 - C_0)^{-1} C_1Y \approx \rho(C_1^{-1}C_0)Y.$

- 1: Generate $g_j^{(k)}$ and $s_j^{(k)}$, $j = 1, \dots, k$ based on (5.3);
 - 2: **for** $j = 1$ to k **do**
 - 3: solve $G_j = S^T Z$ with $\mu = s_j^{(k)}$ according to (5.6) and (5.7);
 - 4: **end for**
 - 5: $\zeta_{c,r,k}(C_1^{-1}C_0)Y = S \sum_{j=1}^k g_j^{(k)} G_j.$
-

with $\text{rank}(M - xN) = \gamma - 1$ for all $x \in \mathbb{C}$ and $\varphi(x) = [\varphi_0(x), \dots, \varphi_{\gamma-1}(x)]^T \neq \mathbf{0}$. The CORK method computes the eigenvalues of the CORK linearization of $\tilde{P}(x)$, given by

$$\mathcal{L}_{\tilde{P}}(x) = \begin{bmatrix} \tilde{A}_0 - x\tilde{B}_0 & \cdots & \tilde{A}_{\gamma-1} - x\tilde{B}_{\gamma-1} \\ & & (M - xN) \otimes I_n \end{bmatrix}, \quad (5.10)$$

using a rational Krylov method that fully exploits its Kronecker structure. For detailed implementation strategies and eigenpair computations of (5.10), we refer to [42].

In our setting, by dividing the first block row of (C_0, C_1) (4.6) by $-k_{\gamma-1}$ and applying the relation $h_{i+1,i} = \frac{k_{i-1}}{k_i}$, we obtain an equivalent representation of P^* consistent with (5.8). Specifically, the coefficients take the form:

$$\tilde{A}_i = A_i - \frac{h_{i+1,\gamma}}{h_{\gamma+1,\gamma}} A_\gamma, \quad i = 0, 1, \dots, \gamma - 1, \quad (5.11)$$

$$\tilde{B}_i = \begin{cases} 0_{n \times n}, & i = 0, 1, \dots, \gamma - 2, \\ -\frac{1}{h_{\gamma+1,\gamma}} A_\gamma, & i = \gamma - 1. \end{cases} \quad (5.12)$$

Furthermore, leveraging the recurrence relation (4.2), we derive

$$\left(H([\gamma], [\gamma - 1])^T - x [I_{\gamma-1} \quad 0_{(\gamma-1) \times 1}] \right) \begin{bmatrix} \vartheta_0(x) \\ \vdots \\ \vartheta_{\gamma-1}(x) \end{bmatrix} = \mathbf{0}. \quad (5.13)$$

This demonstrates that our linearization for matrix polynomials expressed in a degree-graded basis naturally fits the CORK framework. Consequently, we can directly utilize the efficient CORK implementation developed in [42] to solve the resulting large-scale matrix pencil (C_0, C_1) .

6 Numerical experiments

In this section, we assess the numerical performance of our proposed algorithm through MATLAB R2024a implementations in double precision arithmetic. All experiments are conducted on a 15.3-inch MacBook Air equipped with an M2 chip and 8GB of memory. We test the method using benchmark problems from [18, 21, 35, 39].

To evaluate the effectiveness of our approach, we compare the computed eigenvalues with those obtained by several state-of-the-art methods:

- Beyn’s method [6] (using the implementation from [18, Figure 5.3]),
- RSI [39] (code available at https://github.com/tang0389/RSI_NLEVP),
- Set-valued AAA [29], and
- NLEIGS [20] (code available at <http://twr.cs.kuleuven.be/research/software/nleps/nleigs.html>).

To further demonstrate the advantages of rational filtering and CORK (implementation at <http://twr.cs.kuleuven.be/research/software/nleps/cork.html>), we include two large-scale NEPs. These test cases allow us to compare both accuracy and computational efficiency when computing eigenpairs using our approach versus MATLAB’s built-in `eig` function.

For clarity, we introduce the following nomenclature for our proposed algorithms.

NEP_MiniMax: It computes eigenpairs by

1. obtaining a rational minimax approximant by `m-d-Lawson` (Algorithm 1) and
2. solving the resulting matrix pencil eigenvalue problem using MATLAB’s built-in `eig` function.

NEP_MiniMax-FILTER: It computes eigenpairs by

1. constructing a rational minimax approximant via `m-d-Lawson` and
2. performing subspace iteration with rational filtering (Algorithm 3) to solve the matrix pencil problem.

NEP_MiniMax-CORK: It computes eigenpairs by

1. constructing a rational minimax approximant via `m-d-Lawson` and
2. applying the CORK method [42] to solve the resulting matrix pencil.

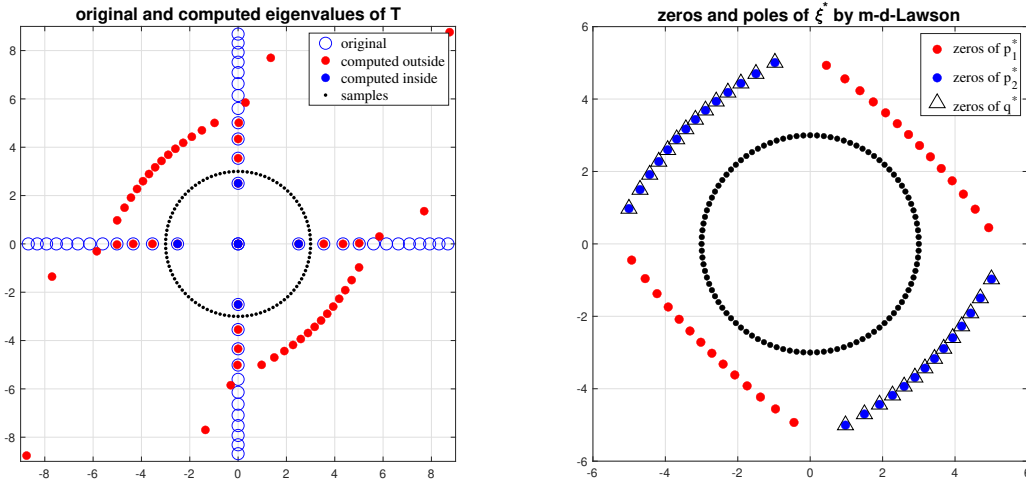


Figure 6.1: The left panel displays eigenvalue computations for (6.1), where blue and red dots represent eigenvalues inside and outside the sampled region (black dots) respectively, obtained via Algorithm 2; original eigenvalues from (6.1) are shown as blue circles for comparison. The right panel plots the poles of ξ^* as triangles, demonstrating that m-d-Lawson produces a numerically best rational approximation— notably pole-free within our region of interest.

Example 6.1. Our first example is from [18, Section 2.1] with

$$T(x) = \begin{bmatrix} e^{ix^2} & 1 \\ 1 & 1 \end{bmatrix}. \quad (6.1)$$

The matrix T becomes singular precisely at the points satisfying $e^{ix^2} = 1$, which occur when $x \in \{\pm\sqrt{2\pi k} : k \in \mathbb{Z}\}$. Consequently, the eigenvalues of T are given by

$$\lambda_k = \pm\sqrt{2\pi k}, \quad k = 0, \pm 1, \pm 2, \dots,$$

with $[1, -1]^T$ serving as a corresponding right eigenvector for every eigenvalue. In our analysis, we focus on the disk $\Omega = \mathcal{D}(0, 3)$ centered at the origin ($c = 0$) with radius $r = 3$, which forms our region of interest.

Within our framework, we construct a set $\mathcal{X} = \{x_\ell\}_{\ell=1}^{100}$ consisting of 100 equidistant sampling points on the circular contour $\mathcal{C}(0, 3) = \{x \in \mathbb{C} : |x| = 3\}$. Using these points with m-d-Lawson, we compute a (28,28)-type rational approximation $\xi^*(x) = \left[\frac{p_1^*(x)}{q^*(x)}, \frac{p_2^*(x)}{q^*(x)} \right]^T$ to $\mathbf{t}(x) = [e^{ix^2}, 1]^T$, achieving an approximation error $\sqrt{e(\xi^*)} < 10^{-10}$. Figure 6.1 (right panel) displays the zeros of $p_1^*(x)$, $p_2^*(x)$, and $q^*(x)$. Remarkably, the reduced form of $\xi^*(x)$ demonstrates that the approximation remains pole-free within our target domain Ω . Consequently, the linearization method developed in Section 4 can be employed to compute eigenvalues of $P^*(x)$ within the target region Ω . Here, we solve the resulting matrix pencil problem using MATLAB's built-in eig function due to its small scale. Each

eigenpair (λ, \mathbf{u}) of P^* computed within Ω is directly treated as a corresponding eigenpair of $T(x)$. Figure 6.1 (left panel) displays the computed eigenvalues of $T(x)$ as blue dots. For completeness, we also show eigenvalues of $P^*(x)$ lying outside Ω as red dots. These results demonstrate that while NEP_MiniMax accurately captures the spectrum of $T(x)$ within Ω , it simultaneously computes additional eigenvalues outside the target region.

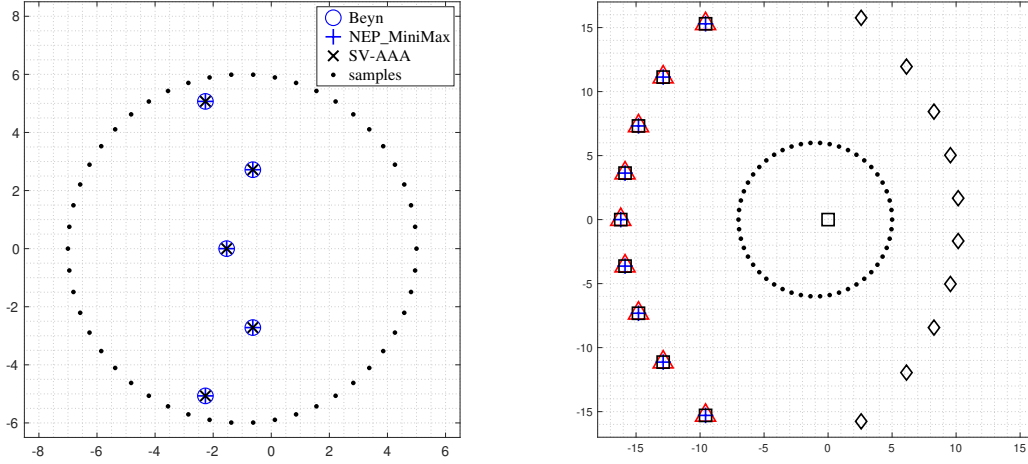


Figure 6.2: Left panel: Computed eigenvalues of (6.2) obtained via NEP_MiniMax (+), Beyn’s method (o), and SV-AAA (x). Right panel: Illustration of poles of ξ^* (\triangle) and zeros of p_1^* (+), p_2^* (\square), and p_3^* (\diamond), computed using m-d-Lawson. Only points with magnitude less than 18 are displayed.

Example 6.2. (Time delay). We consider the example in [35, Example 1] where

$$T(x) = -B_0 + xI + e^{-\tau x} A_1, \quad (6.2)$$

with

$$B_0 = \begin{bmatrix} -5 & 1 \\ 2 & -6 \end{bmatrix}, \quad A_1 = \begin{bmatrix} 2 & -1 \\ -4 & 1 \end{bmatrix}, \quad \tau = 1.$$

This problem is also contained in the NLEVP collection [5] under the name `time_delay2`.

In this example, we use NEP_MiniMax to compute eigenvalues of $T(x)$ within the disk $\mathcal{D}(-1, 6)$ (centered at $c = -1$ with radius $r = 6$). For the approximation, we collect 50 equiangular samples on $\mathcal{C}(-1, 6)$ and construct the set \mathcal{X} . Applying m-d-Lawson, we obtain a (10,10)-type vector-valued rational approximant $\xi^*(x) = \frac{1}{q^*(x)}[p_1^*(x), p_2^*(x), p_3^*(x)]^T$ to $\mathbf{t}(x) = [1, x, e^{-x}]^T$, achieving an approximation error $\sqrt{e(\xi^*)} < 10^{-7}$. The right panel of Figure 6.2 plots the zeros and poles of $\xi^*(x)$, confirming its pole-free property within the disk. Also, we compute eigenvalues of the rational matrix $R^*(x) = \frac{1}{q^*(x)}(-p_1^*(x)B_0 + p_2^*(x)I_2 + p_3^*(x)A_1)$ via linearization, yielding eigenvalue approximations for $T(x)$, as shown in the left panel of Figure 6.2.

For comparison, we compute eigenvalues within $\mathcal{D}(-1, 6)$ using Beyn’s integral method [1] and set-valued AAA (SV-AAA) [2]. In Beyn’s method, we use the numerical quadrature nodes \mathcal{X} (i.e., 50 equispaced points in trapezoid rule) as moment-computation points and fix the probing matrix to a single column (see [18, Section 5] for details). For SV-AAA, we increase the boundary sampling density by a factor of two and iteratively select 11 support points (corresponding to a type (10, 10) rational approximation for $T(x)$) to ensure an approximation error below 10^{-8} . Table 6.1 compares the relative residuals $\epsilon(\lambda, \mathbf{u})$ of the eigenpairs obtained via NEP_MiniMax, Beyn’s method, and SV-AAA, where

$$\epsilon(\lambda, \mathbf{u}) = \frac{\|T(\lambda)\mathbf{u}\|_2}{\|\mathbf{u}\|_2}. \quad (6.3)$$

Table 6.1: Relative residuals $\epsilon(\lambda, \mathbf{u})$ for Example 6.2

relative residuals $\epsilon(\lambda, \mathbf{u})$	eig-index 1	eig-index 2	eig-index 3	eig-index 4	eig-index 5
NEP_MiniMax	2.3660e-09	3.1122e-11	5.2727e-10	8.3716e-11	2.8457e-09
Beyn’s method	4.9460e-06	3.0185e-04	3.9748e-05	3.0185e-04	4.9460e-06
SV-AAA	2.4814e-09	1.4055e-09	1.9067e-10	4.1219e-09	7.6956e-09

Example 6.3. (Hadelers problem). We next consider the Hadelers problem [11, 21] where

$$T(x) = (e^x - 1)B_1 + x^2B_2 - B_0, \quad (6.4)$$

with the coefficient matrices

$$B_0 = b_0 I_n, \quad B_1 = [b_{ij}^{(1)}], \quad B_2 = [b_{ij}^{(2)}],$$

$$b_{ij}^{(1)} = (n + 1 - \max\{i, j\})ij, \quad b_{ij}^{(2)} = n\delta_{ij} + \frac{1}{i + j},$$

and $n = 200$ and $b_0 = 100$.

The eigenvalues of (6.4) are all real, consisting of n negative and n positive values. These eigenvalues become more uniformly spaced farther from the origin, with the smallest eigenvalue near -48 . Following [35], we compute the eigenvalues within the circular region $\Omega = \mathcal{D}(-30, 11.5)$. We discretize the boundary $\mathcal{C}(-30, 11.5)$ using 50 equidistant points to form the approximation set \mathcal{X} . Applying m-d-Lawson, we obtain a degree-6 vector-valued rational approximant $\boldsymbol{\xi}^*(x)$ for $\mathbf{t}(x) = [-1, x^2, e^x - 1]^T$, achieving $\sqrt{e(\boldsymbol{\xi}^*)} < 10^{-10}$. Crucially, $\boldsymbol{\xi}^*(x)$ remains pole-free in $\mathcal{D}(-30, 11.5)$. Finally, we solve the resulting 1200×1200 pencil $C_0 - \lambda C_1$ to compute the eigenvalues.

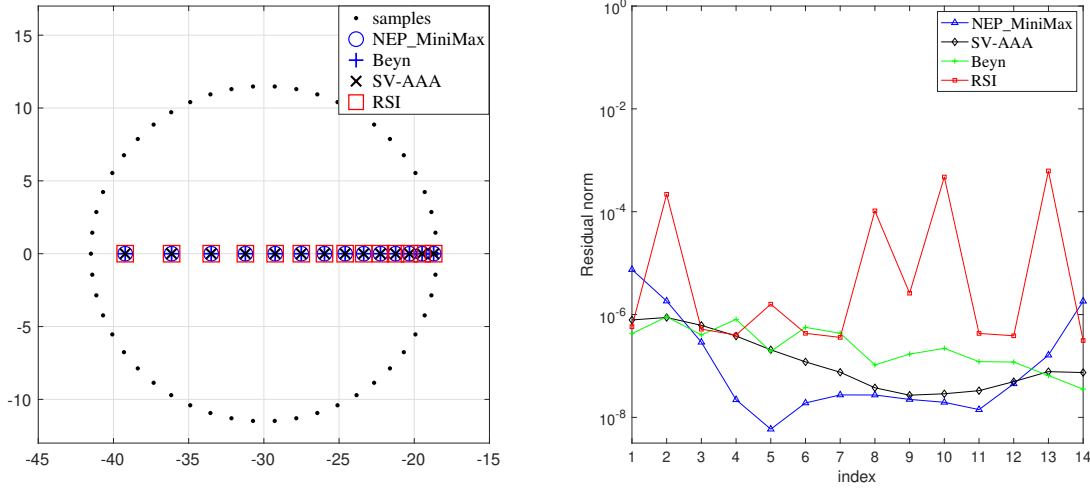


Figure 6.3: Left: Eigenvalues of (6.4) computed via NEP_MiniMax (o), Beyn’s method (+), SV-AAA (x), and RSI (□) are displayed. Right: Relative residuals $\epsilon(\lambda, \mathbf{u})$ of the eigenpairs obtained from NEP_MiniMax, Beyn’s method, SV-AAA, and RSI in Example 6.3.

To facilitate comparison with RSI [35], Beyn’s method, and SV-AAA [29], we begin by computing eigenvalues using NEP_MiniMax. Figure 6.3 displays these numerical results together with their corresponding relative residuals $\epsilon(\lambda, \mathbf{u})$ (6.3) for eigenpairs located within Ω .

We observe that the relative residuals $\epsilon(\lambda, \mathbf{u})$ computed via NEP_MiniMax can be improved by increasing the approximation degree in m-d-Lawson. Higher degrees yield smaller $\sqrt{e(\boldsymbol{\xi}^*)}$, which, according to Corollary 3.1, further reduces $\epsilon(\lambda, \mathbf{u})$. To numerically validate the estimation formula (3.3), Figure 6.4 (left) compares

- the actual relative residuals from NEP_MiniMax using rational approximations of degrees 6, 7, and 8,
- their corresponding a priori estimates $\sqrt{\|\mathcal{G}_{\{E_i\}_i}\|_2 \cdot e(\boldsymbol{\xi}^*)}$, where $\sqrt{\|\mathcal{G}_{\{E_i\}_i}\|_2} = 1.0282 \times 10^8$.

The results confirm the validity of Corollary 3.1 and demonstrate that increasing the approximation degree consistently reduces the relative residuals.

In this example, we evaluate the performance of NEP_MiniMax-FILTER for comparison, as the pencil’s non-trivial scale warrants such analysis. Following the strategy in [9] (adapted for the original NEP via Remark 4.2), we verify the convergence of rational-filter subspace iteration (Algorithm 3) using two thresholds $0 < \tau_r < \tau_g$. An eigenpair (λ, \mathbf{v}) of (C_0, C_1) with relative residual $\varsigma_{c,r}(\lambda, \mathbf{v}) \geq \tau_g$ is classified as a ghost eigenpair, where

$$\varsigma_{c,r}(\lambda, \mathbf{v}) := \frac{\|T(\lambda)\mathbf{v}_1\|_2}{(|c| + r)\|\mathbf{v}_1\|_2}, \quad c = -30, \quad r = 11.5,$$

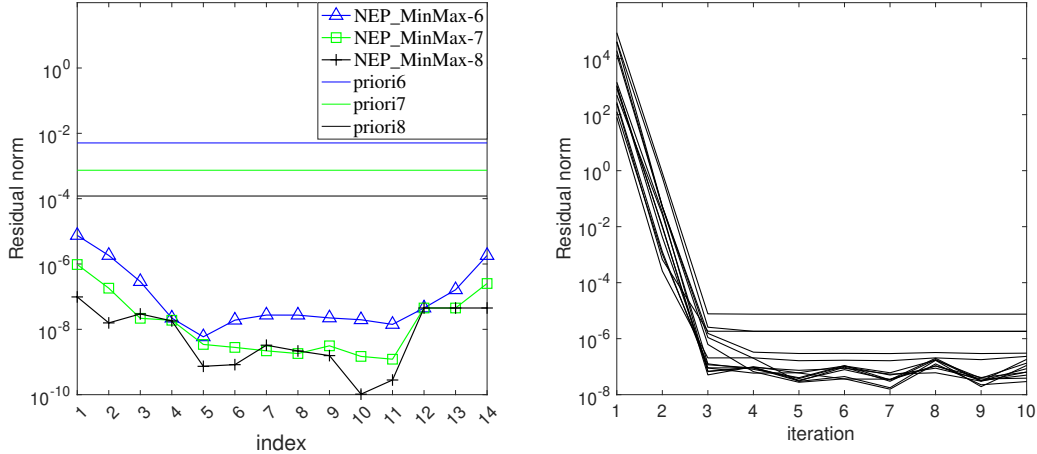


Figure 6.4: Left: Actual relative residuals of the eigenpairs computed by NEP_MiniMax using rational approximations of degrees 6, 7, and 8, along with their corresponding a priori estimates $\sqrt{\|\mathcal{G}_{\{E_i\}_i}\|_2} \epsilon(\boldsymbol{\xi}^*)$. Here, NEP_MiniMax-6 refers to the computation where m-d-Lawson produces a type (6,6) rational approximation, followed by linearization and eigenvalue extraction (priori6 denotes the a priori estimate for NEP_MiniMax-6; analogous conventions apply to degrees 7 and 8). Right: Evolution of residuals $\epsilon(\lambda, \mathbf{u})$ for eigenpairs in Ω over the first 10 iterations of NEP_MiniMax-FILTER-6.

and \mathbf{v}_1 comprises the first n rows of \mathbf{v} . For this example, we set $\tau_r = 10^{-4}$ and $\tau_g = 10^{-2}$. The right panel of Figure 6.4 displays the residuals $\epsilon(\lambda, \mathbf{v}_1) = (|c|+r)\zeta_{c,r}(\lambda, \mathbf{v})$ for eigenpairs in Ω during the first 10 iterations of the subspace method with a degree 6 filter. The results show that NEP_MiniMax-FILTER attains accuracy comparable to NEP_MiniMax within just 5 iterations. Additionally, experiments reveal a significant runtime (including the time of m-d-Lawson) reduction from 12 seconds (NEP_MiniMax) to 3 seconds for this case.

Example 6.4. (Gun problem). We finally examine the “gun” problem, a large-scale model of a radio-frequency gun cavity described by the nonlinear eigenvalue problem with

$$T(x) = K - xM + i\sqrt{x - \sigma_1^2}W_1 + i\sqrt{x - \sigma_2^2}W_2, \quad (6.5)$$

where M , K , W_1 , and W_2 are symmetric 9956×9956 matrices from [18, 28]. The complex square root $\sqrt{\cdot}$ uses the principal branch. Following [5, 28], we set $\sigma_1 = 0$ and $\sigma_2 = 108.8774$. Our computational target consists of the 20 eigenvalues nearest to 250^2 that lie within the upper half-disk Ω centered at $c = 250^2$ with radius $r = 300^2 - 200^2$.

We assess the performance of NEP_MiniMax-CORK in this example. The m-d-Lawson method employs equiangular sampling with 1000 discrete points \mathcal{X} along $\partial\Omega$ to generate a type (6,6) rational approximation $\boldsymbol{\xi}^*(x) = [r_1^*(x), r_2^*(x), r_3^*(x), r_4^*(x)]^T$ for $\mathbf{t}(x) = [1, -x, i\sqrt{x}, i\sqrt{x - \sigma_2^2}]^T$. This approximation yields a structured 6×9956 linearization $C_0 - \lambda C_1$ via Kronecker products, whose eigenvalues within Ω coincide with those of $R^*(x) = r_1^*(x)K + r_2^*(x)M + r_3^*(x)W_1 + r_4^*(x)W_2$, provided $\boldsymbol{\xi}^*(x)$ has no poles in Ω . The

CORK framework is then used to solve the linearized problem (see [42] for implementation specifics). Figure 6.5 displays the poles of $\xi^*(x)$ alongside the eigenvalues of $T(x)$ computed via NEP_MiniMax-CORK within Ω , compared against NLEIGS results. Notably, NEP_MiniMax-CORK terminates in under 4 seconds (including the time of m-d-Lawson), demonstrating its efficiency in locating all eigenvalues of the gun problem in Ω .

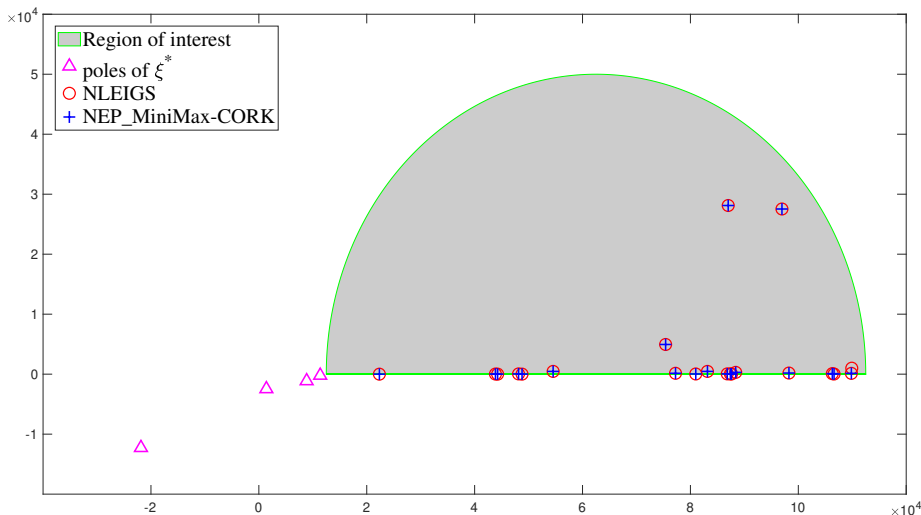


Figure 6.5: This figure displays the computed eigenvalues of the gun problem (6.5) within the region of interest, obtained via NLEIGS (marked with red \circ) and NEP_MiniMax-CORK (shown as blue $+$), along with the poles of $\xi^*(\lambda)$ (indicated by \triangle). The results confirm that $\xi^*(\lambda)$ remains pole-free throughout the region of interest.

Figure 6.6 presents the convergence history of the normalized residual $\varrho_{\text{gun}}(\lambda, \mathbf{u})$ for eigenpairs of $T(x)$ (6.5) computed via NEP_MiniMax-CORK. The implementation uses

- maximum subspace dimension 50,
- $p = 35$ selected Ritz values per restart, and
- cyclically repeated shifts in rational Krylov steps,

where the normalized residual is defined as

$$\varrho_{\text{gun}}(\lambda, \mathbf{u}) = \frac{\|T(\lambda)\mathbf{u}\|_2}{\|K\|_1 + |\lambda| \cdot \|M\|_1 + \sqrt{|\lambda - \sigma_1^2|} \cdot \|W_1\|_1 + \sqrt{|\lambda - \sigma_2^2|} \cdot \|W_2\|_1}. \quad (6.6)$$

The results show that all 20 eigenvalues closest to 250^2 were computed to a tolerance of 10^{-7} in fewer than 80 iterations (4 seconds, including the runtime of m-d-Lawson).

We present a comparative analysis of eigenvalue computation methods by evaluating the residuals $\varrho_{\text{gun}}(\lambda, \mathbf{u})$ (6.6) for 20 eigenpairs obtained from NEP_MiniMax, SV-AAA-EIGS, and NLEIGS at approximation degrees 5, 6, and 7. For SV-AAA-EIGS, we adopt

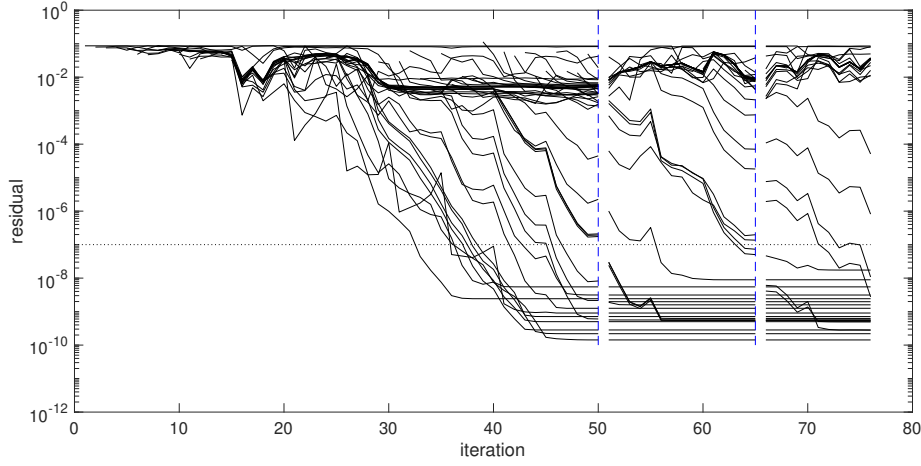


Figure 6.6: The convergence history of the residuals $\varrho_{\text{gun}}(\lambda, \mathbf{u})$ (6.6) of the computed eigenpairs to $T(x)$ (6.5) via NEP_MiniMax-CORK with maximum subspace dimension 50 and 35 selected Ritz values in every restart.

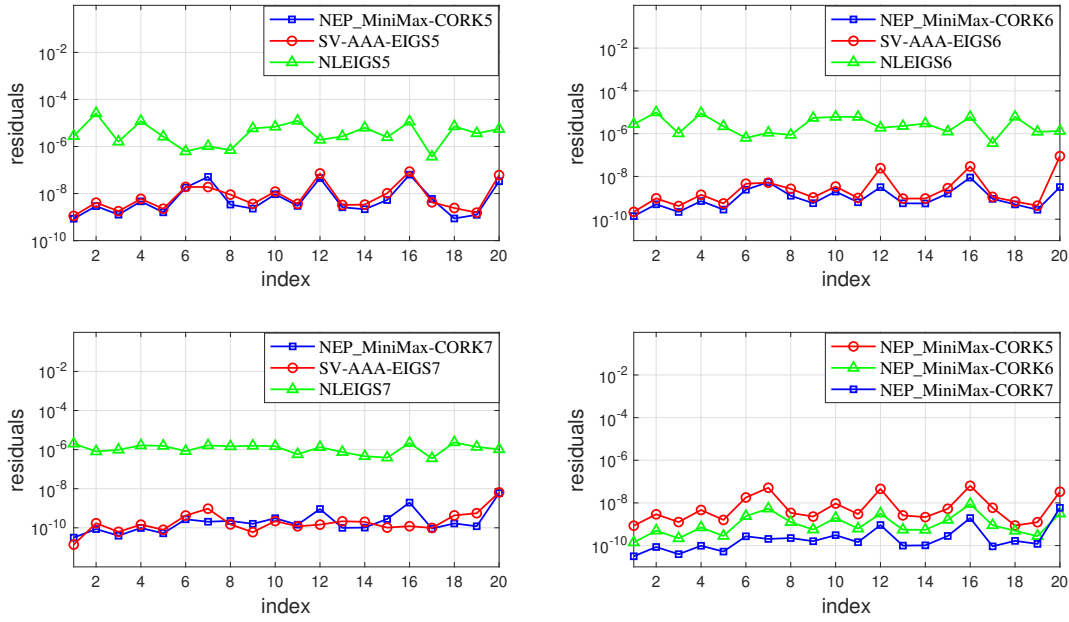


Figure 6.7: The residuals $\varrho_{\text{gun}}(\lambda, \mathbf{u})$ of the computed eigenpairs are shown in the top-left, bottom-left, and top-right panels for NEP_MiniMax-CORK, SV-AAA-EIGS, and NLEIGS at approximation degrees 5, 6, and 7 respectively. The bottom-right panel demonstrates how increasing the approximation degree further reduces the residuals obtained via NEP_MiniMax.

the scheme from [29], constructing the target set from 500 random points within the semi-disk as well as 500 uniformly distributed boundary points. Figure 6.7 demonstrates that `NEP_MiniMax` achieves smaller residuals than `NLEIGS` (comparable to `SV-AAA-EIGS`) at identical approximation degrees. The figure’s lower-right panel shows that increasing the approximation degree further reduces `NEP_MiniMax`’s residuals.

7 Conclusion

In this paper, we presented `NEP_MiniMax`, a novel method for solving nonlinear eigenvalue problems that combines rational minimax approximation via the `m-d-Lawson` algorithm with a new strong linearization framework adaptable to `V+A` polynomial bases while preserving eigenvalue multiplicities. The approach integrates efficiently with scalable eigensolvers through a shift-invert scheme incorporating compact rational Krylov (`CORK`) methods and subspace iteration with rational filters. Numerical experiments demonstrate that `NEP_MiniMax` achieves competitive or superior residual norms compared to existing methods like Beyn’s method, `NLEIGS` and `SV-AAA` at equivalent approximation degrees, with rigorous a priori error bounds linking eigenpair residuals to minimax approximation errors. While our examples focus on moderate-degree approximations where the method shows particular efficiency, we note the expected computational trade-offs for very high-degree cases—a characteristic shared across polynomial-based `NEP` solvers. The method’s distinctive advantages lie in its uniform approximation guarantees and structured preservation of problem properties throughout the solution process.

References

- [1] A. Amiraslani, R. M. Corless and P. Lancaster, Linearization of matrix polynomials expressed in polynomial bases, *IMA J. Numer. Anal.*, **29** (2009), 141–157.
- [2] J. Asakura, T. Sakurai, H. Tadano, T. Ikegami and K. Kimura, A numerical method for nonlinear eigenvalue problems using contour integral, *JSIAM Letters*, **1** (2009), 52–55.
- [3] M. Berljafa and S. Güttel, Generalized rational Krylov decompositions with an application to rational approximation, *SIAM J. Matrix Anal. Appl.*, **36** (2015), 894–916, URL <https://doi.org/10.1137/140998081>.
- [4] M. Berljafa and S. Güttel, The RKFIT algorithm for nonlinear rational approximation, *SIAM J. Sci. Comput.*, **39** (2017), A2049–A2071, URL <https://doi.org/10.1137/15M1025426>.

- [5] T. Betcke, N. Higham, V. Mehrmann, C. Schröder and F. Tisseur, NLEVP: A collection of nonlinear eigenvalue problems, *ACM Trans. Math. Software*, **29** (2013), 1–28.
- [6] W.-J. Beyn, An integral method for solving nonlinear eigenvalue problems, *Linear Algebra Appl.*, **436** (2012), 3839–3863.
- [7] M. C. Brennan, M. Embree and S. Gugercin, Contour integral methods for nonlinear eigenvalue problems: A systems theoretic approach, *SIAM Rev.*, **65** (2023), 439–470.
- [8] P. D. Brubeck, Y. Nakatsukasa and L. N. Trefethen, Vandermonde with Arnoldi, *SIAM Rev.*, **63** (2021), 405–415.
- [9] Y. Chen and Y. Li, Interior eigensolver based on rational filter with composite rule, *SIAM J. Matrix Anal. Appl.*, **46** (2025), 1037–1060, URL <https://doi.org/10.1137/24M1654713>.
- [10] A. A. Condori, Maximum principles for matrix-valued analytic functions, *Amer. Math. Monthly*, **127** (2020), 331–343.
- [11] M. El-Guide, A. Miedlar and Y. Saad, A rational approximation method for solving acoustic nonlinear eigenvalue problems, *Eng. Anal. Bound. Elem.*, **111** (2020), 44–54, URL <https://www.sciencedirect.com/science/article/pii/S0955799719306125>.
- [12] J. K. Eric Polizzi, *FEAST Eigenvalue Solver v3.0 User Guide*, Technical report, 2015, URL arxiv.org/pdf/1203.4031v3.
- [13] C. K. Garrett, Z. Bai and R.-C. Li, A nonlinear QR algorithm for banded nonlinear eigenvalue problems, *ACM Trans. Math. Software*, **43** (2016), 4:1–4:19.
- [14] B. Gavin, A. Miedlar and E. Polizzi, FEAST eigensolver for nonlinear eigenvalue problems, *J. Comput. Sci.*, **27** (2018), 107–117.
- [15] G. H. Golub and C. F. Van Loan, *Matrix Computations*, 4th edition, Johns Hopkins University Press, Baltimore, Maryland, 2013.
- [16] I. V. Gosea and S. Güttel, Algorithms for the rational approximation of matrix-valued functions, *SIAM J. Sci. Comput.*, **43** (2021), A3033–A3054, URL <https://doi.org/10.1137/20M1324727>.
- [17] B. Gustavsen, Matrix Fitting Toolbox, 2009, <https://www.sintef.no/en/software/vector-fitting/downloads/matrix-fitting-toolbox/>.

- [18] S. Güttel and F. Tisseur, The nonlinear eigenvalue problem, *Acta Numer.*, **26** (2017), 1–94.
- [19] S. Güttel, E. Polizzi, P. T. P. Tang and G. Viaud, Zolotarev quadrature rules and load balancing for the FEAST eigensolver, *SIAM J. Sci. Comput.*, **37** (2015), A2100–A2122, URL <https://doi.org/10.1137/140980090>.
- [20] S. Güttel, R. Van Beeumen, K. Meerbergen and W. Michiels, NLEIGS: A class of fully rational Krylov methods for nonlinear eigenvalue problems, *SIAM J. Sci. Comput.*, **36** (2014), A2842–A2864.
- [21] K. P. Hadeler, Mehrparametrische und nichtlineare eigenwertaufgaben, *Arch. Rational Mech. Anal.*, **27** (1967), 306–328, URL <https://doi.org/10.1007/BF00281717>.
- [22] J. M. Hokanson, Multivariate rational approximation using a stabilized Saathanan-Koerner iteration, 2020, URL [arXiv:2009.10803v1](https://arxiv.org/abs/2009.10803v1).
- [23] D. Kressner, A block Newton method for nonlinear eigenvalue problems, *Numer. Math.*, **114** (2009), 355–372.
- [24] V. N. Kublanovskaja, On an application of Newton’s method to the determination of eigenvalues of λ -matrices, *Soviet Math. Dokl.*, **10** (1969), 1240–1241.
- [25] P. Lancaster, A generalised rayleigh quotient iteration for lambda-matrices, *Arch. Rational Mech. Anal.*, **8** (1961), 309–322.
- [26] P. Lancaster, *Lambda-matrices and vibrating systems*, Dover Publications, Inc., Mineola, NY, 2002.
- [27] P. Lancaster, Linearization of regular matrix polynomials, *Electron. Trans. Numer. Anal.*, **17** (2008), 21–27.
- [28] B.-S. Liao, Z. Bai, L.-Q. Lee and K. Ko, Nonlinear Rayleigh–Ritz iterative method for solving large scale nonlinear eigenvalue problems, *Taiwanese J. Math.*, **14** (2010), 869–883.
- [29] P. Lietaert, K. Meerbergen, J. Pérez and B. Vandereycken, Automatic rational approximation and linearization of nonlinear eigenvalue problems, *IMA J. Numer. Anal.*, **42** (2022), 1087–1115.
- [30] Y. Liu, J. E. Roman and M. Shao, Improving performance of contour integral-based nonlinear eigensolvers with infinite GMRES, *SIAM J. Sci. Comput.*, **47** (2025), B595–B617.

- [31] D. S. Mackey, N. Mackey, C. Mehl and V. Mehrmann, Structured polynomial eigenvalue problems: Good vibrations from good linearizations, *SIAM J. Matrix Anal. Appl.*, **28** (2006), 1029–1051.
- [32] D. S. Mackey, N. Mackey, C. Mehl and V. Mehrmann, Vector spaces of linearizations for matrix polynomials, *SIAM J. Matrix Anal. Appl.*, **28** (2006), 971–1004.
- [33] A. Neumaier, Residual inverse iteration for the nonlinear eigenvalue problem, *SIAM J. Numer. Anal.*, **22** (1985), 914–923.
- [34] A. Ruttan, A characterization of best complex rational approximants in a fundamental case, *Constr. Approx.*, **1** (1985), 287–296.
- [35] Y. Saad, M. El-Guide and A. Miedlar, *A rational approximation method for the nonlinear eigenvalue problem*, Technical report, 2020, URL <https://arxiv.org/abs/1901.01188v2>.
- [36] T. Sakurai and H. Sugiura, A projection method for generalized eigenvalue problems using numerical integration, *J. Comput. Appl. Math.*, **159** (2003), 119–128.
- [37] K. Schreiber, *Nonlinear eigenvalue problems: Newton-type methods and nonlinear Rayleigh functionals*, PhD thesis, Technische Universität, Berlin, 2008, URL <http://www.math.tu-berlin.de/~schreibe/>.
- [38] Y. Su and Z. Bai, Solving rational eigenvalue problems via linearization, *SIAM J. Matrix Anal. Appl.*, **32** (2011), 201–216, URL <https://doi.org/10.1137/090777542>.
- [39] Z. Tang and Y. Saad, A rational-Chebyshev projection method for nonlinear eigenvalue problems, *Numer. Linear Algebra Appl.*, **31** (2024), e2563, URL <https://onlinelibrary.wiley.com/doi/abs/10.1002/nla.2563>.
- [40] L. N. Trefethen, *Approximation Theory and Approximation Practice, Extended Edition*, SIAM, 2019.
- [41] R. Van Beeumen, K. Meerbergen and W. Michiels, A rational Krylov method based on Hermite interpolation for nonlinear eigenvalue problems, *SIAM J. Sci. Comput.*, **35** (2013), A327–A350, URL <https://doi.org/10.1137/120877556>.
- [42] R. Van Beeumen, K. Meerbergen and W. Michiels, Compact rational Krylov methods for nonlinear eigenvalue problems, *SIAM J. Matrix Anal. Appl.*, **36** (2015), 820–838, URL <https://doi.org/10.1137/140976698>.
- [43] H. Voss, A Jacobi-Davidson method for nonlinear and nonsymmetric eigenproblems, *Computers & Structures*, **85** (2007), 1284–1292.

- [44] J. L. Walsh, The existence of rational functions of best approximation, *Trans. Amer. Math. Soc.*, **33** (1931), 668–689.
- [45] J. L. Walsh, *Interpolation and Approximation by Rational Functions in the Complex Domain*, 5th edition, Amer. Math. Soc. Colloq. Publ., vol 20, R.I. USA, 1969.
- [46] L. Yang, L.-H. Zhang and Y. Zhang, The Lq-weighted dual programming of the linear Chebyshev approximation and an interior-point method, *Adv. Comput. Math.*, 50:80 (2024).
- [47] G. Yin, A harmonic FEAST algorithm for non-hermitian generalized eigenvalue problems, *Linear Algebra Appl.*, **578** (2019), 75–94.
- [48] G. Yin, R. H. Chan and M.-C. Yeung, A FEAST algorithm with oblique projection for generalized eigenvalue problems, *Numer. Linear Algebra Appl.*, **24** (2017), e2092.
- [49] L.-H. Zhang and S. Han, A convergence analysis of Lawson’s iteration for computing polynomial and rational minimax approximations, *SIAM J. Numer. Anal.*, **63** (2025), 2249–2271.
- [50] L.-H. Zhang, Y. Su and R.-C. Li, Accurate polynomial fitting and evaluation via Arnoldi, *Numerical Algebra, Control and Optimization*, **14** (2024), 526–546.
- [51] L.-H. Zhang, L. Yang, W. H. Yang and Y.-N. Zhang, A convex dual problem for the rational minimax approximation and Lawson’s iteration, *Math. Comp.*, **94** (2025), 2457–2494, DOI: <https://doi.org/10.1090/mcom/4021>.
- [52] L.-H. Zhang, Optimality conditions for rational minimax approximations: Bridging Ruttan’s criteria to dual-based methods, 2026, URL <https://arxiv.org/abs/2602.07862v1>.
- [53] L.-H. Zhang, Y.-N. Zhang, L. Yang and R.-W. Xiao, A AAA-type algorithm for the microwave duplexer filtering, *Numer. Algorithms*, **101** (2025), 1607–1631, <https://doi.org/10.1007/s11075-025-02058-0>.
- [54] L.-H. Zhang, Y.-N. Zhang, C. Zhang and S. Han, Rational minimax approximation of matrix-valued functions, 2025, URL <https://arxiv.org/pdf/2508.06378v2>.
- [55] L.-H. Zhang and Y. Zhang, b-d-Lawson: a method for the interpolation constrained rational minimax approximation, URL <https://arxiv.org/pdf/2502>.
- [56] W. Zhu and Y. Nakatsukasa, Convergence and near-optimal sampling for multivariate function approximations in irregular domains via Vandermonde with Arnoldi, *IMA J. Numer. Anal.*, URL <https://arxiv.org/pdf/2301.12241v2>.